Inorg. Chem. **2006**, *45*, 8907–8921

Highly Phosphorescent Iridium Complexes Containing Both Tridentate Bis(benzimidazolyl)-benzene or -pyridine and Bidentate Phenylpyridine: Synthesis, Photophysical Properties, and Theoretical Study of Ir-Bis(benzimidazolyl)benzene Complex

Shinya Obara,[†] Masumi Itabashi,[†] Fumio Okuda,[§] Satoru Tamaki,[†] Yoshiaki Tanabe,[†] Youichi Ishii,[†] Koichi Nozaki,*[,‡] and Masa-aki Haga*[,†]

Department of Applied Chemistry, Faculty of Science and Engineering, Chuo University, 1-13-27, Kasuga, Bunkyo-ku, Tokyo 112-8551, Japan, Department of Chemistry, Graduate School of Science, Osaka University, 1-16, Machikaneyama, Toyonaka, Osaka 560-0043, Japan, and Central Research Laboratories, Idemitsu Kosan Co., Ltd., 1280 Kami-Izumi, Sodegaura, Chiba 299-293, Japan

Received May 10, 2006

Novel mixed-ligand Ir(III) complexes, $[Ir(L)(N\wedge C)X]^{n+}$ (L = N∧C∧N or N∧N∧N; X = Cl, Br, I, CN, CH_3CN, or –CCPh; $n = 0$ or 1), were synthesized, where N∧C∧N = bis(*N*-methylbenzimidazolyl)benzene (Mebib) and bis(*N*-phenylbenzimidazolyl)benzene (Phbib), N∧N∧N = bis(*N*-methylbenzimidazolyl)pyridine (Mebip), and N∧C = phenylpyridine (ppy) derivatives. The X-ray crystal structures of [Ir(Phbib)(ppy)Cl] and [Ir(Mebib)(mppy)Cl] [mppy = 5-methyl-2-(2′-pyridyl)phenyl] indicate that the nitrogen atom of the ppy ligand is located trans to the coordinating carbon atom in Me- or Phbib, while the coordinating carbon atom in ppy occupies the trans position of Cl. $[Ir(Mebip)(ppy)Cl]^+$ showed a quasireversible Ir(III/IV) oxidation wave at +1.05 V, while the Ir complexes, [Ir(Mebib)(ppy)Cl], were oxidized at +0.42 V versus Fc/Fc^+. The introduction of an Ir–C bond in [Ir(Mebib)(ppy)Cl] induces a large potential shift of 0.63 V in a negative direction. Further, the oxidation potential of [Ir(Mebib)(Rppy)X] was altered by the substitution of R, R′, and X groups. Compared to the oxidation potential, the first reduction potential revealed an almost constant value at –2.36 to –2.46 V for [Ir(L)(ppy)Cl] (L = Mebib and Phbib) and –1.52 V for [Ir(Mebip)(ppy)Cl. The UV–vis spectra of [Ir(Mebib)(R-ppy)X] show a clear singlet metal-to-ligand charge-transfer transition around 407∼425 nm and a triplet metal-to-ligand charge-transfer transition at 498∼523 nm. $[Ir(Mebip)(ppy)Cl]^+$ emits at 610 nm with a luminescent quantum yield of $\Phi = 0.16$ at room temperature. The phosphorescence of [Ir(Mebib)(ppy)X] was observed at 526 nm for X = CN and 555 nm for X = Cl with the high luminescent quantum yields, $\Phi = 0.77\sim0.86$, at room temperature. [Ir(Phbib)(ppy)Cl] shows the emission at 559 nm with a luminescent quantum yield of $\Phi = 0.95$, which is an unprecedentedly high value compared to those of other emissive metal complexes. Compared to the luminescent quantum yields of the $Ir(ppy)_2(L)$ derivatives and $[Ir(Mebip)(ppy)Cl]^+$, the neutral Ir complexes, [Ir(L)(R-ppy)X] (L = Me- or Phbib), reveal very high quantum yields and large radiative rate constants (k_r) ranging from 3.4×10^5 to 5.5×10^5 s^{-1}. The density functional theory calculation suggests that these Ir complexes possess dominantly metal-to-ligand charge-transfer and halide-to-ligand charge-transfer excited states. The mechanism for a high phosphorescence yield in [Ir(bib)(ppy)X] is discussed herein from the perspective of the theoretical consideration of radiative rate constants using perturbation theory and a one-center spin–orbit coupling approximation.

Introduction

The design of luminescent inorganic compounds continues to attract great interest in the development of organic light-emitting diodes (OLEDs).[1,2] It has recently been demonstrated that luminescent cyclometalated Ir(III) complexes such as $Ir(ppy)_3$ and $Ir(ppy)_2(acac)$ (ppy = phenylpyridinate and acac = acetylacetonate) may serve as triplet-emitting dopants for constructing OLEDs.[3−13] A significant research

* Authors to whom correspondence should be addressesd. Phone: 81 3-3817-1908. Fax: 81 3-3817-1895. E-mail: mhaga@chem.chuo-u.ac.jp (M.-a.H.) and nozaki@ch.wani.osaka-u.ac.jp (K.N.).
[†] Chuo University.
[‡] Osaka University.
[§] Idemitsu Kosan Co., Ltd.

(1) Baldo, M. A.; O'Brien, D. F.; Shoustrikov, A.; Sibley, S.; Thompson, M. E.; Forrest, S. R. *Nature* **1998**, *395*, 151.
(2) Baldo, M. A.; Thompson, M. E.; Forrest, S. R. *Nature* **2000**, *403*, 750.

10.1021/ic060796o CCC: $33.50
Published on Web 09/29/2006

Chart 1. Examples of Ir Complexes with Tridentate Ligands

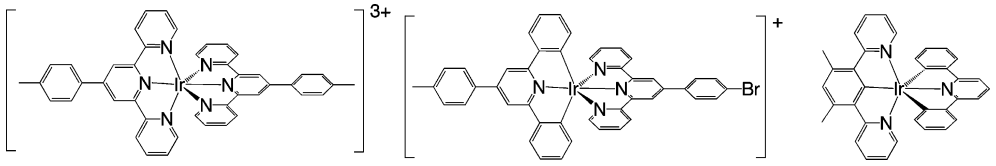

effort has been made to improve the internal quantum efficiency of OLEDs by use of Ir(III) cyclometalated complexes with high luminescence quantum yields. As a consequence, many bis- and tris-cyclometalated complexes of Ir(III) with relatively high quantum efficiency (~0.5) have been synthesized. Recently, $[Ir(ppy)_2(X)_2]^-$ (X = CN, NCS, and NCO) have been reported to exhibit unprecedentedly high quantum yields (~1);[14] however, these results are puzzling because of the inability of other groups, including us, to reproduce the data. On the other hand, only limited examples of luminescent Ir(III) complexes with tridentate ligands are known (Chart 1).[15−20]

The octahedral Ir complexes can be classified in categories by the coordination atoms around the Ir ion, that is, $Ir(N)_6$ type for $[Ir(tpy)_2]^{3+}$, $Ir(N)_5X$ for $[Ir(tpy)(bpy)Cl]^{2+}$, $Ir(N)_4(C)_2$ for $[Ir(bpy)(ppy)_2]^+$, $Ir(N)_3(C)_3$ for $[Ir(ppy)_3]$, $Ir(N)_2(C)_2(O)_2$ for $[Ir(ppy)_2(acac)]$, $Ir(N)_3(C)_2O$ for $[Ir(ppy)_2(pic)]$, and so forth. The coordination environment around the Ir(III) ion strongly affects the Ir 5d orbital energy, and the excited-state properties of Ir complexes are governed by the orbital mixing between Ir 5d and ligand π^* orbitals. In particular, the introduction of an Ir−C bond leads to a stronger ligand field on the Ir ion, which induces the destabilization of Ir 5d orbitals; as a result, there is larger state mixing of the metal-to-ligand charge-transfer (MLCT) excited state with ligand-centered ones. We have recently synthesized the $Ir(N)_6$- and $Ir(N)_5(C)$-type Ir complexes, $[Ir(Mebip)_2]^{3+}$ and $[Ir(Mebip)(Mebib)]^{2+}$ [Mebip = bis(*N*-methyl-2-benzimidazolyl)pyridine and Mebib = bis(*N*-methyl-2-benzimidazolyl)benzene].[21,22] The mixed-ligand complex, $[Ir(Mebip)(Mebib)]^{2+}$, showed a higher luminescence quantum yield than the $Ir(N)_6$-type complex, $[Ir(Mebip)_2]^{3+}$. Furthermore, the comparison of the emission quantum yields for $[Ir(Mebip)_2]^{3+}$, $[Ir(Mebip)(Mebib)]^{2+}$, and $[Ir(Mebip)(bpy)Cl]^{2+}$ revealed that the mixed-ligand coordination environments of the Ir ion surrounded by both tridentate and bidentate ligands lead to higher-emission quantum yields.

Therefore, the judicious selection of coordination atoms and an appropriate ligand π-orbital system hold the key to facilitating the development of highly emissive Ir complexes. We report herein the synthesis and photophysical properties of highly luminescent $Ir(N)_3(C)_2(X)$-type Ir(III) complexes containing both tridentate N∧C∧N and bidentate N∧C ligands, as shown in Chart 2. For comparison, the corresponding $Ir(N)_4(C)(X)$-type complex, $[Ir(Mebip)(ppy)X]^+$, was also synthesized.

Chart 2. Chemical Structures of Ligands, Their Ir Complexes, and Their Numbering[a]

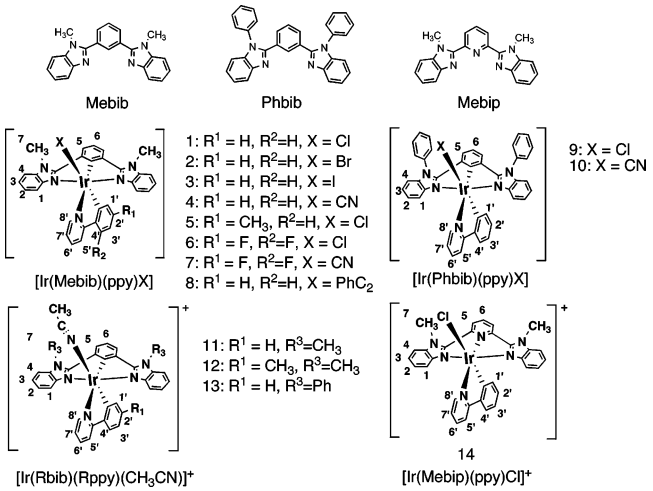

[a] The abbreviation of ligands and the proton-numbering system is also shown for the assignment of ^{1}H NMR spectra.

Experimental Section

Materials. Isophthalic acid (Aldrich), NH_4PF_6 (Wako), 1-phenyl-2-(trimethylsilyl)acethylene (Aldrich), $Pd(PPh_3)_4$ (Kanto), 2,4-difluorophenylbronic acid (Aldrich), pyridine dicarboxylic acid

(3) Lamansky, S.; Djurovich, P.; Murphy, D.; Abdel-Razzaq, F.; Lee, H.-E.; Adachi, C.; Burrows, P. E.; Forrest, S. R.; Thompson, M. E. *J. Am. Chem. Soc.* **2001**, *123*, 4304−4312.
(4) Huang, W. S.; Lin, J. T.; Chien, C. H.; Tao, Y. T.; Sun, A. S.; Wen, Y. S. *Chem. Mater.* **2004**, *16*, 2480.
(5) Jenmifer, B. M.; Rayabarapu, D. K.; Cheng, C. H. *Adv. Mater.* **2004**, *16*, 2480.
(6) Chen, T. M.; Laskar, I. R. *Chem. Mater.* **2004**, *16*, 111.
(7) Cheng, C. H.; Sun, P. P.; Duan, J. P. *Adv. Mater.* **2003**, *15*, 224.
(8) Sun, I. W.; Tai, C. C.; Yang, C. H. *J. Mater. Chem.* **2004**, *14*, 947.
(9) Tsuboyama, A.; Iwawaki, H.; Furugori, M.; Mukaide, T.; Kamatani, J.; Igawa, S.; Moriyama, T.; Miura, S.; Takiguchi, T.; Okada, S.; Hoshino, M.; Ueno, K. *J. Am. Chem. Soc.* **2003**, *125*, 12971−12979.
(10) Tamayo, A. B.; Alleyne, B. D.; Djurovich, P. I.; Lamansky, S.; Tsyba, I.; Ho, N. N.; Bau, R.; Thompson, M. E. *J. Am. Chem. Soc.* **2003**, *125*, 7377−7387.
(11) Grushin, V. V.; Herron, N.; LastName, D. L.; Marshell, W. J.; Petrov, V. A.; Wang, Y. *Chem. Commun.* **2001**, 1494.
(12) Li, J.; Djurovich, P. I.; Alleyne, B. D.; Yousufuddin, M.; Ho, N. N.; Thomas, J. C.; Peters, J. C.; Bau, R.; Thompson, M. E. *Inorg. Chem.* **2005**, *44*, 1713.
(13) Hwang, F.-M.; Chen, H.-Y.; Chen, P.-S.; Liu, C.-S.; Chi, Y.; Shu, C.-F.; Wu, F.; Chou, P.-T.; Peng, S.-M.; Lee, G.-H. *Inorg. Chem.* **2005**, *44*, 1344.
(14) Nazeeruddin, M. K.; Humphry-Baker, R.; Berner, D.; Rivier, S.; Zuppiroli, L.; Graetzel, M. *J. Am. Chem. Soc.* **2003**, *125*, 8790−8797.
(15) Collin, J. P.; Dixon, I. M.; Sauvage, J. P.; Williams, J. A. G.; Barigelletti, F.; Flamigni, L. *J. Am. Chem. Soc.* **1999**, *121*, 5009.
(16) Lo, K. K. W.; Chung, C. K.; Ng, D. C. M.; Zhu, N. *New. J. Chem.* **2002**, *26*, 81.
(17) Yoshikawa, N.; Matumura-Inoue, T. *Anal. Sci.* **2003**, *19*, 761.
(18) Polson, M.; Fracasso, S.; Bertolasi, V.; Ravaglia, M.; Scandola, F. *Inorg. Chem.* **2004**, *43*, 1950.
(19) Wilkinson, J. A.; Goeta, A. E.; Foster, C. E.; Williams, J. A. G. *Inorg. Chem.* **2004**, *43*, 6513.
(20) Neve, F.; Crispini, A.; Serroni, S.; Loiseau, F.; Campagna, S. *Inorg. Chem.* **2001**, *40*, 1093.
(21) Yutaka, T.; Obara, S.; Ogawa, S.; Nozaki, K.; Ikeda, N.; Ohno, T.; Ishii, Y.; Sakai, K.; Haga, M.-a. *Inorg. Chem.* **2005**, *44*, 4737−4746.
(22) Yutaka, T.; Obara, S.; Haga, M.; Yokoyama, Y.; Sakai, K. *Acta Crystallogr., Sect. E* **2005**, *61*, m1357−m1359.

(Aldrich), *N*-methyl-1,2-phenylenediamine (Aldrich), 2-(*p*-tolyl)-pyridine (mppy) (Aldrich), and $IrCl_3 \cdot nH_2O$ (Heraeus) were used as received. The other synthetic reagents were purchased from Kanto Kagaku and used as received. For the photophysical measurements, dichloromethane, acetonitrile, *N*,*N*-dimethylformamide (spectroscopic grade), methanol, and ethanol (HPLC grade) were purchased from Kanto Kagaku and used as received. For the electrochemical measurements, *N*,*N*-dimethylformamide for non-aquesous titrimetry (Kanto) was used as supplied, and tetra-*n*-butylammonium tetrafluoroborate (Nacalai) was purified by recrystallization from EtOH. Ir(Mebip)Cl_3, 2-(4′,6′-difluorophenyl)pyridine (dfppy), Mebib, Mebip,[23] and 2,6-bis(1-phenylbenzimidazol-2-yl)benzene (Phbib)[7] were prepared according to the literature.

Synthesis. [Ir(Mebib)Cl_2]$_2$. $IrCl_3 \cdot 4H_2O$ (0.10 g, 0.27 mmol) and Mebib (0.183 g, 0.54 mmol) were refluxed in methanol (15 mL) for 5 h. After cooling to room temperature, the resulting precipitate was collected and washed with methanol and then ether. This complex is insoluble in common organic solvents and was therefore used without purification for further preparation. Yield: 0.13 g (82%). Anal. Calcd for $[C_{22}H_{17}N_4IrCl_2]_2$: C, 44.00; H, 2.85; N, 9.33. Found: C, 43.98; H, 3.00; N, 9.72. MALDI-MS: *m*/*z* 1201.91 (1201.09 required for $[C_{44}H_{35}N_8Ir_2Cl_4]^+$).

[Ir(Phbib)Cl_2]$_2$. This complex was synthesized in a manner similar to that for [Ir(Mebib)Cl_2]$_2$, except that bis(*N*-phenylbenzimidazolyl)benzene (Phbib) was used instead of Mebib. A pale yellow precipitate was obtained. This complex was used as a starting compound for the next reaction without further purification. Yield: 66%.

[Ir(Mebib)(ppy)Cl]. The mixture of [Ir(Mebib)Cl_2]$_2$ (0.1 g, 0.084 mmol) and ppy (0.46 g, 1.4 mmol) in glycerol (30 mL) was irradiated in a microwave (650 W, multimode) for 6 min. After the mixture cooled to room temperature, water (50 cm^3) was added to give a yellow-orange precipitate. After the precipitate was filtered and washed with hexane and ether, an orange precipitate was obtained. Yield: 0.03 g (23%). Anal. Calcd for $C_{33}H_{25}N_5IrCl$: C, 55.11; H, 3.50; N, 9.74. Found: C, 54.86; H, 3.60; N, 9.85. ^{1}H NMR ($CDCl_3$): δ 4.29 (s, 6H, N-*Me*), 5.84 (d, 1H, J = 7.0 Hz, $H_{1'}$), 6.26 (d, 2H, J = 8.0 Hz, H_1), 6.47 (t, 1H, J = 6.9 Hz, $H_{2'}$), 6.60 (t, 1H, J = 7.5 Hz, $H_{3'}$), 6.91 (t, 2H, J = 7.5 Hz, H_2), 7.15 (t, 2H, J = 7.5 Hz, H_3), 7.24 (d, 2H, J = 8.0 Hz, H_4), 7.39 (t, 1H, J = 8.0 Hz, H_6), 7.50 (d, 1H, J = 8.0 Hz, $H_{4'}$), 7.64 (t, 1H, J = 7.0 Hz, $H_{7'}$), 7.97 (d, 2H, J = 7.5 Hz, H_5), 8.10 (m, 2H, $H_{5',6'}$), 10.61 (d, 1H, J = 5.7 Hz, $H_{8'}$). ESI MS: *m*/*z* 719.405 (719.143 required for $[C_{33}H_{25}N_5IrCl]^+$).

[Ir(Mebib)(ppy)Br]. [Ir(Mebib)(ppy)Cl] (0.05 g, 0.07 mmol) and NaBr (0.0215 g, 0.35 mmol) were heated by microwave irradiation (650 W) in ethylene glycol (20 cm^3) for 6 min. After the mixture was cooled to room temperature, the addition of water resulted in the formation of an orange precipitate, which was collected by filtration and washed with water and ether. The purification was performed by recrystallization from CH_2Cl_2−hexane. Yield: 0.034 g (64%). Anal. Calcd for $C_{33}H_{25}N_5IrBr$: C, 51.90; H, 3.30; N, 9.17. Found: C, 51.86; H, 3.60; N, 9.35. ^{1}H NMR ($CDCl_3$): δ 4.29 (s, 6H, N-*Me*), 5.79 (d, 1H, J = 7.4 Hz, $H_{1'}$), 6.26 (d, 2H, J = 8.6 Hz, H_1), 6.47 (t, 1H, J = 7.4 Hz, $H_{2'}$), 6.60 (t, 1H, J = 7.4 Hz, $H_{3'}$), 6.91 (t, 2H, J = 7.7 Hz, H_2), 7.15 (t, 2H, J = 7.4 Hz, H_3), 7.23 (m, 2H, H_4), 7.38 (t, 1H, J = 7.7 Hz, H_6), 7.49 (d, 1H, J = 7.4 Hz, $H_{4'}$), 7.62 (t, 1H, J = 6.9 Hz, $H_{7'}$), 7.98 (d, 2H, J = 7.4 Hz, H_5), 8.11 (m, 2H, $H_{5',6'}$), 10.81 (d, 1H, J = 6.3 Hz, $H_{8'}$).

(23) Addison, A. W.; Burke, P. J. *J. Heterocycl. Chem.* **1981**, *18*, 803−805.

[Ir(Mebib)(ppy)I]. The synthetic procedure was the same as that used for [Ir(Mebib)(ppy)Br], substituting NaBr for NaI. Yield: 50%. Anal. Calcd for $C_{33}H_{25}N_5IrI$: C, 48.89; H, 3.11; N, 8.64. Found: C, 48.41; H, 3.30; N, 8.85. ^{1}H NMR ($CDCl_3$): δ 4.23 (s, 6H, N-*Me*), 5.61 (d, 1H, J = 6.9 Hz, $H_{1'}$), 6.20 (d, 1H, J = 8.0 Hz, H_1), 6.42 (t, 1H, J = 8.3 Hz, $H_{2'}$), 6.54 (t, 1H, J = 8.0 Hz, $H_{3'}$), 6.85 (t, 2H, J = 8.3 Hz, H_2), 7.09 (t, 2H, J = 7.7 Hz, H_3), 7.17 (2H, m, H_4), 7.31 (t, 1H, J = 7.7 Hz, H_6), 7.39 (d, 1H, J = 9.2 Hz, $H_{4'}$), 7.52 (t, 1H, J = 7.2 Hz, $H_{7'}$), 7.94 (d, 2H, J = 7.4 Hz, H_5), 8.03 (m, 2H, $H_{5',6'}$), 11.01 (d, 1H, J = 5.2 Hz, $H_{8'}$).

[Ir(Mebib)(ppy)(CN)]. [Ir(Mebib)(ppy)Cl] (0.05 g, 0.07 mmol) and KCN (0.0091 g, 0.14 mmol) were heated by microwave irradiation (650 W) in ethylene glycol (10 cm^3) for 5 min. After the mixture was cooled to room temperature, the addition of water resulted in the formation of a yellow precipitate, which was collected by filtration and washed with water and ether. The purification was performed by recrystallization from CH_2Cl_2−hexane. Yield: 0.03 g (61%). Anal. Calcd for $C_{34}H_{25}N_6Ir$: C, 57.53; H, 3.55; N, 11.84. Found: C, 57.75; H, 3.33; N, 11.45. ^{1}H NMR ($CDCl_3$): δ 4.20 (s, 6H, N-*Me*), 5.79 (d, 1H, J = 6.3 Hz, $H_{1'}$), 6.19 (d, 2H, J = 8.0 Hz, H_1), 6.48 (t, 1H, J = 7.5 Hz, $H_{2'}$), 6.60 (t, 1H, J = 6.3 Hz, $H_{3'}$), 6.86 (t, 2H, J = 8.0 Hz, H_2), 7.09 (d, 2H, J = 8.0 Hz, H_3), 7.19 (t, 2H, J = 8.0 Hz, H_6), 7.35 (t, 1H, J = 7.5 Hz, $H_{5'}$), 7.47 (d, 1H, J = 8.0 Hz, $H_{7'}$), 7.91 (d, 2H, J = 7.5 Hz, H_5), 8.03 (d, 2H, J = 4.5 Hz, $H_{5',6'}$), 10.48 (d, 1H, J = 5.7 Hz, $H_{1'}$). FT-IR (KBr): 2102.6 cm^{-1} [ν(CN)]. MALDI MS: *m*/*z* 710.07 (710.18 required for $[C_{34}H_{25}N_6Ir]^+$).

[Ir(Mebib)(dfppy)Cl]. The mixture of [Ir(Mebib)Cl_2]$_2$ (0.1 g, 0.084 mmol) and dfppy (0033 g, 0.17 mmol) in glycerol (10 cm^3) was irradiated with a microwave (650 W, multimode) for 4 min under a nitrogen atmosphere. After the mixture cooled to room temperature, water (50 cm^3) was added to give the yellow-orange precipitate. The precipitate was collected by filtration and washed with hexane and ether. Purification was performed by the diffusion of ether to a CH_2Cl_2 solution of the complex. Yield: 0.046 g (32%). Anal. Calcd for $C_{33}H_{23}N_5IrClF_2$: C, 52.48; H, 3.07; N, 9.27. Found: C, 52.12; H, 3.43; N, 9.55. ^{1}H NMR ($CDCl_3$): δ 4.25 (s, 6H, N-*Me*), 5.27 (d, 1H, J = 9.5 Hz, $H_{1'}$), 6.02 (t, 1H, J = 10.5 Hz, $H_{3'}$), 6.12 (d, 2H, J = 8.6 Hz, H_1), 6.88 (t, 2H, J = 7.5 Hz, H_2), 7.12 (t, 2H, J = 7.5 Hz, H_3), 7.21 (d, 2H, J = 8.0 Hz, H_4), 7.34 (t, 1H, J = 8.0 Hz, H_6), 7.58 (t, 1H, J = 7.5 Hz, $H_{7'}$), 7.91 (d, 2H, J = 7.5 Hz, H_5), 8.04 (t, 1H, J = 8.6 Hz, $H_{6'}$), 8.41 (d, 1H, J = 8.6 Hz, $H_{5'}$), 10.57 (d, 1H, J = 5.7 Hz, $H_{8'}$). ^{19}F NMR ($CDCl_3$): δ −110.0, −110.6. ESI MS: *m*/*z* 755.411 (755.123 required for $[C_{33}H_{23}N_5F_2IrCl]^+$).

[Ir(Mebib)(mppy)Cl]·2CH_2Cl_2. The synthetic procedure was the same as that used for the [Ir(Mebib)(dfppy)Cl] analogue, substituting dfppy for mppy. Orange crystals suitable for X-ray analysis were obtained by the diffusion of ether to a CH_2Cl_2 solution of the complex. Yield: 32%. Anal. Calcd for $C_{34}H_{27}N_5IrCl \cdot 2CH_2Cl_2$: C, 47.88; H, 3.46; N, 7.75. Found: C, 47.65; H, 3.20; N, 7.89. ^{1}H NMR ($CDCl_3$): δ 1.85 (s, 3H, Ph-Me), 4.29 (s, 6H, N-Me), 5.62 (s, 1H, $H_{1'}$), 6.26 (d, 2H, J = 8.0 Hz, H_1), 6.40 (d, 1H, J = 6.3 Hz, $H_{3'}$), 6.90 (t, 2H, J = 7.5 Hz, H_2), 7.13 (t, 2H, J = 8.0 Hz, H_3), 7.22 (t, 2H, J = 8.0 Hz, H_4), 7.37 (t, 2H, J = 7.0 Hz, H_6), 7.58 (t, 1H, J = 7.0 Hz, $H_{7'}$), 7.96 (d, 2H, J = 7.5 Hz, H_5), 8.04 (m, 2H, $H_{5',6'}$), 10.56 (d, 1H, J = 5.1 Hz, $H_{8'}$). ESI MS: *m*/*z* 733.175 (733.155 required for $[C_{34}H_{27}N_5IrCl]^+$).

[Ir(Mebib)(dfppy)CN]. The complex was synthesized in a manner similar to that for [Ir(Mebib)(ppy)CN]. Yield: 72%. Anal. Calcd for $C_{34}H_{23}N_6IrF_2$: C, 54.76; H, 3.11; N, 11.27. Found: C, 54.42; H, 3.50; N, 11.52. ^{1}H NMR ($CDCl_3$): δ 4.30 (s, 6H, N-*Me*), 5.31 (d, 1H, J = 8.2 Hz, $H_{1'}$), 6.09 (t, 1H, J = 10.0 Hz, $H_{3'}$), 6.18

(d, 1H, $J = 8.0$ Hz, H_1), 6.95 (t, 2H, $J = 7.5$ Hz, H_2), 7.19 (t, 2H, $J = 7.5$ Hz, H_3), 7.29 (d, 2H, $J = 8.0$ Hz, H_4), 7.42 (t, 1H, $J = 8.0$ Hz, H_6), 7.57 (t, 1H, $J = 7.2$ Hz, $H_{7'}$), 7.98 (d, 2H, $J = 7.5$ Hz, H_5), 8.12 (t, 1H, $J = 7.5$ Hz, $H_{6'}$), 8.45 (d, 1H, $J = 9.8$ Hz, $H_{5'}$), 10.55 (d, 1H, $J = 4.6$ Hz, $H_{8'}$). FT-IR (KBr): 2105.8 cm^{-1} [ν-(CN)]. MALDI MS: *m*/*z* 745.95 (746.16 required for $[C_{34}H_{23}N_6F_2Ir]^+$).

[Ir(Mebib)(mppy)(CH$_3$CN)](OTf). The complex was synthesized in a manner similar to that for [Ir(Mebib)(ppy)(CH$_3$CN)](OTf), except that [Ir(Mebib)(mppy)Cl] (0.051 g, 0.07 mmol) was used as a starting compound. Yield: 88%. Anal. Calcd for $C_{37}H_{30}N_6IrF_3SO_3$: C, 50.05; H, 3.40; N, 9.46. Found: C, 49.63; H, 3.90; N, 10.07. ^{1}H NMR ($CDCl_3$): δ 1.79 (s, 3H, Ph-*Me*), 4.37 (s, 6H, N-*Me*), 5.58 (s, 1H, $H_{1'}$), 6.16 (d, 2H, $J = 8.6$ Hz, H_1), 6.49 (t, 2H, $J = 8.0$ Hz, $H_{2'}$), 7.03 (t, 2H, $J = 7.5$ Hz, H_2), 7.30 (t, 2H, $J = 7.5$ Hz, H_3), 7.48 (d, 1H, $J = 7.5$ Hz, $H_{4'}$), 7.56 (d, 2H, $J = 8.0$ Hz, H_4), 7.61 (t, 1H, $J = 8.0$ Hz, H_6), 7.76 (t, 1H, $J = 6.0$ Hz, $H_{7'}$), 8.20 (d, 2H, $J = 8.0$ Hz, H_5), 8.28 (m, 2H, $H_{5',6'}$), 9.79 (d, 1H, $J = 4.0$ Hz, $H_{8'}$). ESI MS: *m*/*z* 739.124 (739.216 required for $[C_{36}H_{30}N_6Ir]^+$).

[Ir(Mebib)(mppy)(CCPh)]. The mixture of KF (20 mg, 0.339 mmol) and Me$_3$Si−CCPh (20 mg, 0.113 mmol) in methanol (10 cm^3) was stirred for 30 min at room temperature under a nitrogen atmosphere. To the solution was added [Ir(Mebib)(mppy)(CH$_3$CN)](OTf) (0.05 g, 0.056 mmol), and the solution was refluxed for 2 h. After the solution cooled to room temperature, a yellow precipitate was formed, which was collected by filtration and washed with methanol and ether. The complex was recrystallized from CH_2Cl_2−ether. Yield: 54%. Anal. Calcd for $C_{42}H_{32}N_5Ir$: C, 63.14; H, 4.04; N, 8.76. Found: C, 62.96; H, 3.72; N, 9.02. ^{1}H NMR ($CDCl_3$): δ 1.72 (s, 3H, Ph-Me), 4.31 (s, 6H, N-*Me*), 5.60 (s, 1H, $H_{1'}$), 6.19 (d, 2H, $J = 8.0$ Hz, H_1), 6.38 (d, 1H, $J = 8.0$ Hz, $H_{2'}$), 6.78 (d, 2H, $J = 6.9$ Hz, C-*Ph*), 6.85 (t, 1H, $J = 7.5$ Hz, C-*Ph*), 6.92 (m, 3H, $J = 8.0$ Hz, C−Ph, H_2), 7.19 (t, 2H, $J = 7.5$ Hz, H_3), 7.45 (m, 4H, $H_{6,4,4'}$), 7.63 (q, 1H, $H_{7'}$), 8.12 (d, 2H, $J = 4.6$ Hz, $H_{5',6'}$), 8.15 (d, 2H, $J = 8.0$ Hz, H_5), 10.69 (d, 1H, $J = 5.7$ Hz, $H_{8'}$). ESI MS: *m*/*z* 799.564 (799.229 required for $[C_{42}H_{32}N_5Ir]^+$).

[Ir(Phbib)(ppy)Cl]. This complex was synthesized in a manner similar to that for [Ir(Mebib)(ppy)Cl], except that Phbib was used instead of Mebib. The crude compound was purified by column chromatography on silica with CH_2Cl_2−methanol (25:1 v/v) and recrystallized from CH_2Cl_2−benzene−hexane. Red crystals were obtained. Yield: 24%. Anal. Calcd for $C_{43}H_{31}N_5IrClO$: C, 59.95; H, 3.63; N, 8.10. Found: C, 59.93; H, 3.46; N, 7.60. ^{1}H NMR ($CDCl_3$-*d*): δ 5.92 (d, 1H, $J = 7.4$ Hz, $H_{1'}$), 6.34 (d, 2H, $J = 8.6$ Hz, H_1), 6.55 (t, 1H, $J = 7.4$ Hz, $H_{2'}$), 6.68 (t, 1H, $J = 7.4$ Hz, $H_{3'}$), 6.74 (m, 3H, *$H_{4,6}$), 6.95 (dt, 4H*, $J = 7.3$ and 3.6 Hz, $H_{2,5}$), 7.07 (t, 2H, $J = 7.4$ Hz, H_3), 7.53 (t, 2H, $J = 3.1$ Hz, N-*Ph*), 7.58 (d, 1H, $J = 8.0$ Hz, $H_{4'}$), 7.60−7.68 (m, 8H, $J = 3.7$ and 1.9 Hz, N-*Ph*), 7.70 (t, 1H, $J = 6.3$ Hz, $H_{7'}$), 8.12 (t, 1H, $J = 7.5$ Hz, $H_{6'}$), 8.17 (d, 1H, $J = 8.0$ Hz, $H_{5'}$), 10.71 (d, 1H, $J = 5.7$ Hz, $H_{8'}$).

[Ir(Phbib)(ppy)CN]·2H$_2$O. The complex was obtained by a metathesis reaction of [Ir(Phbib)(ppy)Cl] with KCN under conditions similar to those for [Ir(Mebib)(ppy)(CN)]. A yellow powder was obtained. Yield: 21.0%. Anal. Calcd for $C_{44}H_{33}N_6IrO_2$: C, 60.74; H, 3.82; N, 9.66. Found: C, 61.03; H, 3.46; N, 9.85. ^{1}H NMR ($CDCl_3$-*d*): δ 5.92 (d, 1H, $J = 7.4$ Hz, $H_{1'}$), 6.35 (d, 2H, $J = 7.4$ Hz, H_1), 6.63 (t, 1H, $J = 7.2$ Hz, $H_{2'}$), 6.72−6.78 (m, 4H, $H_{3',4,6}$), 6.97 (dt, 4H, $J = 7.4$ and 3.7 Hz, $H_{2,5}$), 7.09 (t, 2H, $J = 8.0$ Hz, H_3), 7.50 (t, 2H, $J = 6.0$ Hz, N-*Ph*), 7.60 (d, 1H, $J = 8.0$ Hz, $H_{4'}$), 7.63−7.72 (m, 9H, $H_{7'}$, N-*Ph*), 8.16 (m, 2H, $H_{5',6'}$), 10.66 (d, 1H, $J = 5.7$ Hz, $H_{8'}$).

[Ir(Mebib)(ppy)(CH$_3$CN)](OTf)·Et$_2$O. [Ir(Mebib)(ppy)Cl] (0.05 g, 0.07 mmol) and AgOTf (0.036 g, 0.14 mmol) in acetonitrile (20 cm^3) were refluxed for 3 h. After the mixture was cooled to room temperature, the solution was filtered through Celite. The resulting yellow filtrate was concentrated in vacuo to one-fourth of its original volume, and the addition of ether afforded the precipitation. The purification was performed by recrystallization from CH_2Cl_2−ether. Yield: 92%. Anal. Calcd for $C_{36}H_{28}N_6IrF_3SO_3$·Et$_2$O: C, 50.68; H, 4.04; N, 8.86. Found: C, 50.26; H, 4.41; N, 8.51. ^{1}H NMR ($CDCl_3$): δ 4.26 (s, 6H, N-*Me*), 5.64 (d, 1H, $J = 8.0$ Hz, $H_{1'}$), 6.06 (d, 2H, $J = 8.0$ Hz, H_1), 6.42 (t, 1H, $J = 8.0$ Hz, $H_{2'}$), 6.58 (t, 1H, $J = 8.0$ Hz, $H_{3'}$), 6.93 (t, 2H, $J = 7.5$ Hz, H_2), 7.20 (t, 2H, $J = 7.5$ Hz, H_3), 7.46 (d, 2H, $J = 8.0$ Hz, H_4), 7.50 (t, 1H, $J = 8.0$ Hz, $H_{4'}$), 7.71 (m, 1H, $H_{7'}$), 8.11 (d, 2H, $J = 8.0$ Hz, H_5), 8.22 (d, 2H, $J = 4.5$ Hz, $H_{5',6'}$), 9.75 (d, 1H, $J = 5.7$ Hz, $H_{8'}$). ESI MS: *m*/*z* 725.132 (725.201 required for $[C_{35}H_{28}N_6Ir]^+$).

[Ir(Phbib)(ppy)(CH$_3$CN)](OTf). The complex was synthesized in a manner similar to that for [Ir(Mebib)(ppy)(CH$_3$CN)](OTf), except [Ir(Phbib)(ppy)Cl] was used as a starting compound. Yield: 30%. Anal. Calcd for $C_{46}H_{32}N_6IrF_3SO_3$: C, 55.36; H, 3.23; N, 8.42. Found: C, 55.00; H, 3.40; N, 8.77. ^{1}H NMR (CD_3CN): δ 5.71 (d, 1H, $J = 7.4$ Hz, $H_{1'}$), 6.24 (d, 2H, $J = 8.0$ Hz, H_1), 6.55 (t, 1H, $J = 6.9$ Hz, $H_{2'}$), 6.71−6.69 (m, 3H, $H_{2,6}$), 6.89 (t, 1H, $J = 8.0$ Hz, $H_{3'}$), 7.07−7.06 (m, 4H, $H_{2,5}$), 7.20 (t, 2H, $J = 7.7$ Hz, H_3), 7.58 (d, 2H, $J = 7.4$ Hz, N-*Ph*), 7.63 (d, 1H, $J = 7.4$ Hz, $H_{4'}$), 7.76−7.69 (m, 8H, N-*Ph*), 7.84 (t, 1H, $J = 5.4$ Hz, $H_{7'}$), 8.32 (dt, 2H, $J = 6.9$ and 3.4 Hz, $H_{5',6'}$), 9.90 (d, 1H, $J = 5.2$ Hz, $H_{8'}$). ESI MS: *m*/*z* 861.06 (861.02 required for $[C_{46}H_{32}N_6Ir]^+$).

[Ir(Mebip)(ppy)Cl](PF$_6$)·2CH$_3$CN. A mixture of [Ir(Mebip)Cl$_3$] (0.1 g, 0.16 mmol) and ppy (0.03 g, 0.19 mmol) in glycerol (30 mL) was irradiated in a microwave (650 W, multimode) for 12 min under a nitrogen atmosphere. After the mixture cooled to room temperature, a saturated aqueous solution of NH_4PF_6 (20 cm^3) was added to give an orange-red precipitate. The resulting precipitate was filtered and washed with hexane, $CHCl_3$, and ether. Single crystals were grown from a slow evaporation of ether into a CH_3CN solution of the complex. The crystals lost solvated Et$_2$O in vacuo. Yield: 0.03 g (61%). Anal. Calcd for $C_{36}H_{31}ClF_6N_8IrP$: C, 45.59; H, 3.29; N, 11.82. Found: C, 45.94; H, 3.10; N, 11.65. ^{1}H NMR (DMSO-d_6): δ 4.59 (s, 6H, N-*Me*), 5.90 (d, 2H, $J = 8.6$ Hz, H_1), 6.08 (d, 1H, $J = 7.5$ Hz, $H_{1'}$), 6.73 (t, 1H, $J = 6.9$ Hz, $H_{2'}$), 6.82 (t, 1H, $J = 7.5$ Hz, $H_{3'}$), 7.20 (t, 2H, $J = 8.0$ Hz, H_2), 7.51 (t, 2H, $J = 7.7$ Hz, H_3), 7.85 (d, 2H, $J = 8.0$ Hz, $H_{4'}$), 7.93 (m, 3H, $H_{4,7'}$), 8.41 (t, 1H, $J = 8.0$ Hz, $H_{6'}$), 8.50 (t, 1H, $J = 8.3$ Hz, H_5), 8.57 (d, 1H, $J = 8.0$ Hz, $H_{5'}$), 8.82 (d, 2H, $J = 8.6$ Hz, H_6), 10.35 (d, 1H, $J = 4.5$ Hz, $H_{8'}$). ESI MS: *m*/*z* 721.52 (721.15 required for $[C_{32}H_{25}N_6IrCl]^+$).

Physical Measurements. ^{1}H NMR, ESI MS, MALDI-TOF MS, and UV−vis spectra were recorded with a Mercury 300 (Varian) or JNM-ECA 500 (JEOL) spectrometer, a Micromass electrospray LCT, and Shimadzu MALDI-TOF AXIMA-CFR mass spectrometer, and a Hewlett-Packard 8453 UV−vis spectrophotometer, respectively. For the assignment of ^{1}H NMR spectra, the proton-numbering system in Chart 1 is used in this paper. Electrochemical measurements were carried out in a standard one-compartment cell under N_2 gas, equipped with a BAS platinum (ϕ 1.6 mm) or a BAS glassy-carbon (ϕ 3 mm) working electrode, a platinum wire counter electrode, and a Ag/Ag^+ reference electrode with an ALS/CH model 660A electrochemical analyzer. The reference electrode was $Ag/AgNO_3$ (0.01 M in 0.1 M $TBABF_4$ CH_3CN), abbreviated as Ag/Ag^+. The ferrocene/ferrocenium (Fc/Fc^+) oxidation process was used as an internal reference standard, and all potentials are reported versus Fc/Fc^+. The $E_{1/2}$ values for the Fc/Fc^+ couple were +0.04

V versus Ag/Ag^+, which was found to be 0.33 V more negative than that versus a saturated calomel electrode. Emission spectra were recorded using a grating monochromator (Triax 1900, Jobin Yvon) with a CCD image sensor (S7031, Hamamatsu). The spectral sensitivity of the spectrofluorometer was corrected using a bromine lamp (IPD 100V 500WCS, Ushio). A sample solution in a 1 mm quartz cell was deoxygenated and excited using an LD-excited solid-state Nd:YAG laser (355 nm, 440 ps, 13 kHz, 6 mW, JDS Uniphase). The emission quantum yields of the Ir(III) compounds were determined using 9,10-diphenylanthracene (DPA; $\Phi = 0.91$) as a reference.[24] Depolarized light was used in all cases to determine emission quantum yields. The error in the emission quantum yields is determined primarily by the accuracy of the sensitivity correction in the spectral range from 450 to 800 nm, which is ±5%. The Huang−Rhys factors of accepting modes were determined by a one-mode Franck−Condon analysis of emission spectra using eq 1 in ref 26b.[25,26]

For the determination of emission lifetimes, the deoxygenated sample solution was photoexcited using a pulsed Nd:YAG laser. The light from the sample was monochromated using a grating monochromator (H-20, Jobin Yvon) and converted into current signals by a photomultiplier tube (R3896, Hamamatsu). The transient signals for 10 240∼2560 shots were accumulated on a digitizing oscilloscope (HP 54520 Hewlett-Packard) to get the decay profile of the emission intensity, which was fit to a single-exponential function with convolution of the instrumental response function of the measuring system. The time resolution of the system was 2 ns.. The measurements at 77 K were performed using a cylindrical quartz cell (1 mm inner diameter) and a liquid-nitrogen Dewar.

Density functional theory (DFT) calculations were performed with the Gaussian 98, revision A11.3, suite (G98)[27] and with the Amsterdam Density Functional program package (ADF, version 2002).[28−30] The basis functions used in the computations with G98 were Dunning−Hay's split-valence double-ζ for C, H, and N atoms (D95) and the Hay−Wadt double-ζ with a Los Alamos relativistic effective core potential for heavy atoms (LANL2DZ).[31,32] Becke's style three-parameter hybrid functional of B3PW91 was employed.[33−35] For the computations with ADF, an uncontracted triple-ζ Slater-type orbital basis set with one polarization function was used (denoted as tzp). The core orbitals (C and N, 1s; Cl, 1s2p; Ir, 1s4d) were obtained as solutions of an all-electron calculation on the isolated atom and kept frozen during the self-consistent field calculation of the molecule. The zero-order regular approximation[36−38] was used for relativistic corrections. Both the local spin density approximation with the parametrization of Vosko, Wilk, and Nusair (VWN)[39] and the generalized gradient approximated correlation functional proposed by Perdew and Wang (PW91) were employed. Drawing of the molecular orbitals was performed using MOLEKEL.[40,41]

X-ray Diffraction Studies for $5\cdot 2CH_2Cl_2$, $9\cdot C_6H_{14}$, $11OTf\cdot Et_2O$, 13OTf, and $14PF_6\cdot 2CH_3CN\cdot 0.5Et_2O$. Red block crystals of [Ir(Mebib)(mppy)Cl]·$2CH_2Cl_2$ (**5**·$2CH_2Cl_2$), yellow block crystals of [Ir(Mebib)(ppy)(CH_3CN)]OTf·Et_2O (**11**OTf·Et_2O), yellow plate crystals of [Ir(Phbib)(ppy)(CH_3CN)]OTf (**13**OTf), orange block crystals of [Ir(Phbib)(ppy)Cl]·C_6H_{14} (**9**·C_6H_{14}), and orange block crystals of [Ir(Mebip)(ppy)Cl]PF_6·$2CH_3CN$·$0.5Et_2O$ (**14**PF_6·$2CH_3CN$·$0.5Et_2O$) were obtained by the slow diffusion of diethyl ether or *n*-hexane into the corresponding dichloromethane or acetonitrile solutions. Diffraction data for **5**·$2CH_2Cl_2$, **11**OTf·Et_2O, **13**OTf, **9**·C_6H_{14}, and **14**PF_6·$2CH_3CN$·$0.5Et_2O$ were collected on a Rigaku Mercury CCD area detector with graphite monochromated Mo Kα radiation ($\lambda = 0.710\,69$ Å) at -150 ± 1 °C for the 2θ range of 5−55°. Intensity data were corrected for numerical absorptions (NUMABS[42] for **14**PF_6·$2CH_3CN$·$0.5Et_2O$) or empirical absorptions (REQAB[43] for **5**·$2CH_2Cl_2$, **11**OTf·Et_2O, **9**·C_6H_{14}, and **13**OTf) and for Lorentz and polarization effects. Corrections for secondary extinction were further applied for **14**PF_6·$2CH_3CN$·$0.5Et_2O$ (coefficient, 0.162 05), for **13**OTf·Et_2O (coefficient, 30.82), and for **9**·C_6H_{14} (coefficient, 148.07).[44] The structure solution and refinements were carried out using the *CrystalStructure* package.[45,46] The positions of the non-hydrogen atoms were determined by heavy-atom Patterson methods (SHELX-97[47] for **14**PF_6·$2CH_3CN$·$0.5Et_2O$ and **5**·$2CH_2Cl_2$; PATTY[48] for **11**OTf·Et_2O) or direct methods

(24) Murov, S. L.; Carmichael, I.; Hug, G. L. *Handbook of Photochemistry*, 2nd ed.; Marcel Dekker: New York, 1993.
(25) Kober, E. M.; Casper, J. V.; Lumpkin, R. S.; Meyer, T. J. *J. Phys. Chem.* **1986**, *90*, 3722−3734.
(26) Islam, A.; Ikeda, N.; Nozaki, K.; Ohno, T. *J. Photochem. Photobiol., A* **1997**, *106*, 61−66.
(27) Frisch, M. J.; Trucks, G. W.; Schlegel, H. B.; Scuseria, G. E.; Robb, M. A.; Cheeseman, J. R.; Zakrzewski, V. G.; Montgomery, J. A.; Stratmann, R. E.; Burant, J. C.; Dapprich, S.; Millam, J. M.; Daniels, A. D.; Kudin, K. N.; Strain, M. C.; Farkas, O.; Tomasi, J.; Barone, V.; Cossi, M.; Cammi, R.; Mennucci, B.; Pomelli, C.; Adamo, C.; Clifford, S.; Ochterski, J.; Petersson, G. A.; Ayala, P. Y.; Cui, Q.; Morokuma, K.; Malick, D. K.; Rabuck, A. D.; Raghavachari, K.; Foresman, J. B.; Cioslowski, J.; Ortiz, J. V.; Stefanov, B. B.; Liu, G.; Liashenko, A.; Piskorz, P.; Komaromi, I.; Gomperts, R.; Martin, R. L.; Fox, D. J.; Keith, T.; Al-Laham, M. A.; Peng, C. Y.; Nanayakkara, A.; Gonzalez, C.; Challacombe, M.; Gill, P. M. W.; Johnson, B. G.; Chen, W.; Wong, M. W.; Andres, J. L.; Head-Gordon, M.; Replogle, E. S.; Pople, J. A. *Gaussian 98*, version A11.3; Gaussian Inc.: Pittsburgh, PA, 1998.
(28) Baerends, E. J.; Ellis, D. E.; Ros, P. *Chem. Phys.* **1993**, *2*, 42.
(29) Boerrigter, P. M.; Velde, G. t.; Baerends, E. J. *Int. J. Quantum Chem.* **1988**, *33*, 87.
(30) Velde, G. t.; Baerends, E. J. *J. Comput. Phys.* **1992**, *99*, 84.
(31) Dunning, T. H., Jr.; Hay, P. J. In *Modern Theoretical Chemistry*; Schaefer, H. F., III, Ed.; Plenum: New York, 1976; Vol. 3.
(32) Hay, P. J.; Wadt, W. R. *J. Chem. Phys.* **1985**, *82*, 270; 284; 299.
(33) Perdew, J. P. *Phys. Rev. B: Condens. Matter Mater. Phys.* **1986**, *33*, 8822.
(34) Perdew, J. P.; Burke, K.; Wang, Y. *Phys. Rev. B: Condens. Matter Mater. Phys.* **1996**, *54*, 16533.
(35) Becke, A. D. *J. Chem. Phys.* **1993**, *98*, 5648.
(36) Lenthe, E.; Baerends, E. J.; Snijders, J. G. *J. Chem. Phys.* **1993**, *99*, 4957.
(37) Lenthe, E.; Ehlers, A. E.; Baerends, E. J. *J. Chem. Phys.* **1999**, *110*, 8943.
(38) Lenthe, E. V.; Leeuwen, R. V.; Baerends, E. J.; Snijders; J. G. *J. Quantum. Chem.* **1996**, *57*, 281.
(39) Vosko, S. H.; Wilk, L.; Nusair, M. *Can. J. Phys.* **1980**, *58*, 1200.
(40) Flukiger, P.; Luthi, H. P.; Portmann, S.; Weber, J. *Swiss Center for Scietific Computing*, Manno, Switzerland, 2000−2002.
(41) Portmann, S.; Luthi, H. P. *Chimia* **2000**, *54*, 766.
(42) Higashi, T. *NUMABS: Numerical Absorption Correction*; Rigaku Corp.: Tokyo, Japan, 1999.
(43) Jacobson, R. A. *REQAB: Private Communication to Rigaku Corp.*; Rigaku Corp.: Tokyo, Japan, 1998.
(44) Larson, A. C. In *Crystallographic Computing*; *Proceedings of an International Summer School Organized by The Commission on Crystallographic Computing of the International Union of Crystallography*, August 4−11, 1969, Ottawa, Canada; Ahmed, F. R., Hall, S. R., Huber, C. P., Eds.; Munksgaard: Copenhagen, Denmark, 1970; pp 291−295.
(45) *CrystalStructure 3.60*: *Single Crystal Structure Analysis Software*; Rigaku Corp: Tokyo, Japan; MSC: The Woodlands, TX, 2000−2004.
(46) Watkin, D. J.; Prout, C. K.; Carruthers, J. R.; Betteridge, P. W. *CRYSTALS Issue 10*; Chemical Crystallography Laboratory: Oxford, U. K., 1996.
(47) Sheldrick, G. M. *SHELX-97*: *Program for the Refinement of Crystal Structure*; University of Göttingen: Göttingen, Germany, 1997.
(48) Beurskens, P. T.; Admiraal, G.; Beurskens, G.; Bosman, W. P.; Garcia-Granda, S.; Gould, R. O.; Smits, J. M. M.; Smykalla, C. *PATTY*: *The DIRDIF Program System*; Technical Report of the Crystallography Laboratory; University of Nijmengen: Nijmengen, The Netherlands, 1992.

Table 1. X-ray Crystallographic Data for **5**·$2CH_2Cl_2$, **9**·C_6H_{14}, **11**OTf·Et_2O, **13**OTf, and **14**PF_6·2MeCN·$0.5Et_2O$

	5·$2CH_2Cl_2$	**9**·C_6H_{14}	**11**OTf·Et_2O	**13**OTf	**14**PF_6·2MeCN·$0.5Et_2O$
chemical formula	$C_{36}H_{31}Cl_5IrN_5$	$C_{49}H_{43}ClIrN_5$	$C_{40}H_{38}F_3IrN_6O_4S$	$C_{46}H_{32}F_3IrN_6O_3S$	$C_{38}H_{36}ClF_6IrN_8O_{0.5}P$
fw	903.16	929.59	948.05	998.07	985.39
cryst color, habit	red, block	orange, block	yellow, block	yellow, plate	orange, block
dimensions of crystal	0.30 × 0.15 × 0.10	0.90 × 0.80 × 0.80	0.50 × 0.40 × 0.20	0.50 × 0.35 × 0.15	0.20 × 0.20 × 0.20
cryst syst	monoclinic	monoclinic	triclinic	monoclinic	monoclinic
space group	$P2_1/c$	$P2_1/c$	$P1$	$C2/c$	$P2_1/c$
a, Å	14.360(6)	10.53(2)	8.94(2)	26.59(3)	11.156(2)
b, Å	14.339(6)	20.44(3)	13.21(2)	10.36(1)	16.503(3)
c, Å	17.123(7)	18.15(5)	16.71(3)	29.29(3)	21.440(4)
α, deg			78.19(8)		
β, deg	107.460(6)	99.04(6)	79.99(11)	99.76(4)	102.924(3)
γ, deg			82.88(9)		
V, Å^3	3363.3(24)	3859.1(14)	1894.9(50)	7951.8(14)	3847.2(13)
Z	4	4	2	8	4
ρ_{calcd}, g cm^{-3}	1.783	1.600	1.661	1.667	1.701
μ, cm^{-1}	44.13	35.82	36.53	34.85	36.62
range of trans. factors	0.6326−1.0000	0.4692−1.0000	0.5335−1.0000	0.5335−1.0000	0.4129−0.5559
no. rflns measured	12694	34574	17204	36271	28274
no. unique rflns	6562	9713	8112	11397	8668
R_{int}	0.090	0.078	0.047	0.056	0.068
no. rflns used	2548 [$I > 3\sigma(I)$]	5407 [$I > 3\sigma(I)$]	6951 [$I > 3\sigma(I)$]	7401 [$I > 3\sigma(I)$]	3052 [$I > 2\sigma(I)$]
no. params refined	430	519	535	573	534
R [$I > 3\ \sigma(I)$][a]	0.055 [$I > 3\sigma(I)$]	0.062 [$I > 3\sigma(I)$]	0.040 [$I > 3\sigma(I)$]	0.048 [$I > 3\sigma(I)$]	0.031 [$I > 2\sigma(I)$]
R_w [$I > 3\ \sigma(I)$][b]	0.056 [$I > 3\sigma(I)$]	0.066 [$I > 3\sigma(I)$]	0.041 [$I > 3\sigma(I)$]	0.050 [$I > 3\sigma(I)$]	0.033 [$I > 2\sigma(I)$]
GOF [$I > 3\ \sigma(I)$][c]	1.002	1.000	1.000	1.000	1.000

[a] $R = \sum||F_o| - |F_c||/\sum|F_o|$. [b] $R_w = [\sum w(|F_o| - |F_c|)^2/\sum wF_o^2]^{1/2}$, $w = [pF_0^2 + q\sigma(F_0^2) + 0.5]^{-1}$ [$p = 0$ (**11**OTf, **12**·C_6H_{14}, **14**PF_6·2MeCN·$0.5Et_2O$), 0.0007 (**5**·$2CH_2Cl_2$), 0.0001 (**11**OTf·Et_2O); $q = 0.185$ (**14**PF_6·2MeCN·$0.5Et_2O$), 1.35 (**5**·$2CH_2Cl_2$), 2.98 (**11**OTf·Et_2O), 2.075 (**9**·C_6H_{14}), 2.033 (**13**OTf)]. [c] GOF $= [\sum w(|F_o| - |F_c|)^2/(N_{obs} - N_{params})]^{1/2}$.

(SHELX-97[47] for **9**·C_6H_{14}; SIR-97[49] for **11**OTf) and subsequent Fourier syntheses (DIRDIF99).[50] For **14**PF_6·$2CH_3CN$·$0.5Et_2O$, the C(10) and C(17) atoms were refined with isotropic parameters, while the solvating Et_2O molecule positioned on the center of symmetry was modeled over two positions with occupancies of 50%. For **5**·$2CH_2Cl_2$, the C(2), C(5), C(10), C(16), and C(18) atoms were refined with isotropic parameters. For **9**·C_6H_{14}, the carbon atoms of *n*-hexane were refined with isotropic parameters. All of the other non-hydrogen atoms were refined on F_o [$I > 2\sigma(I)$ for **14**PF_6·$2CH_3CN$·$0.5Et_2O$; $I > 3\sigma(I)$ for the others] by full-matrix least-squares techniques with anisotropic thermal parameters, while all of the hydrogen atoms were placed at the calculated positions (C−H distance of 0.95 Å) with fixed isotropic parameters. The atomic scattering factors were taken from ref 51. Anomalous dispersion effects were included in F_c.[52] The values of $\Delta f'$ and $\Delta f''$ were taken from refs 53 and 54. The maximum and minimum residual peaks on the final difference Fourier maps were 0.63/−0.63, 0.78/−0.88, 1.14/−1.47, 2.66/−2.43, and 2.27/−1.73 for **14**PF_6·$2CH_3CN$·$0.5Et_2O$, **5**·$2CH_2Cl_2$, **11**OTf·Et_2O, **9**·C_6H_{14}, and **13**OTf, respectively. Details of the X-ray diffraction study are summarized in Table 1, and selected bond lengths, bond angles, and selected torsion angles between planes are listed in Tables 1S and 2S in the Supporting Information.

Results and Discussion

Syntheses and Characterizations. The reaction of Mebib or Phbib with $IrCl_3$·$4H_2O$ in methanol gave an insoluble yellow precipitate (**P**), of which MALDI-TOF mass spectrometry provides the mass peak corresponding to $[Ir_2(L)_2Cl_4]^+$ (L = Mebib or Phbib). Because the compound was insoluble in common organic solvents and water, this compound **P** was used as a starting material without further characterization. The corresponding Rh(III) complexes have been synthesized by the reaction of ligand L with $RhCl_3$·$3H_2O$, in which the insoluble product might be formulated as $[Rh_2(L)_2X_4]$ (L = Hbib and Mebib; X = Cl, Br, and I) by FAB-MS and ^{1}H NMR for $[Rh_2(Hbib)_2Cl_4]$ in DMSO-d_6.[55] New mixed-ligand Ir(III) complexes with the coordination environment of [Ir(L)(N∧C)Cl] (L = N∧N∧N and N∧C∧N) were prepared by the reaction of compound **P** with the N∧C ligand under microwave irradiation conditions in glycerol, where Mebip, Me- or Phbib, and ppy were used as N∧N∧N, N∧C∧N, and N∧C, respectively (see Chart 1). As for [Ir(L)(N∧C)Cl], two geometrical isomers are possible because N∧C is coordinated to Ir in an asymmetrical manner; that is, two isomers are shown in Chart 3 as an example of [Ir(Mebib)(ppy)Cl].

When the reaction took place in ethylene glycol under reflux conditions for 15 h, the reaction product gave a complicated NMR spectrum, which arose from the formation of a mixture of the two isomers. However, upon microwave

(49) Altomare, A.; Burla, M.; Camalli, M.; Cascarano, G.; Giacovazzo, C.; Guagliardi, A.; Moliterni, A.; Polidori, G.; Spagna, R. *J. Appl. Crystallogr.* **1999**, *32*, 115−119.
(50) Beurskens, P. T.; Admiraal, G.; Beurskens, G.; Bosman, W. P.; de Gelder, R.; Israel, R.; Smits, J. M. M. *DIRDIF99: The DIRDIF-99 Program System*; Technical Report of the Crystallography Laboratory; University of Nijmegen: Nijmengen, The Netherlands, 1999.
(51) Cromer, D. T.; Waber, J. T. *International Tables for X-ray Crystallography*; Ibers, J. A., Hamilton, W. C., Eds.; Kynoch Press: Birmingham, England, 1974; Vol. IV, Table 2.2 A.
(52) Ibers, J. A.; Hamilton, W. C. *Acta Crystallogr.* **1964**, *17*, 781.
(53) Creagh, D. C.; McAuley, W. J. *International Tables for X-ray Crystallography*; Wilson, A. J. C., Ed.; Kluwer Academic Publishers: Boston, MA, 1992; Vol. C, Table 4.2.6.8.
(54) Creagh, D. C.; Hubbell, J. H. *International Tables for X-ray Crystallography*; Wilson, A. J. C., Ed.; Kluwer Academic Publishers: Boston, MA, 1992; Vol. C, Table 4.2.4.3.
(55) Gayathri, V.; Leelamani, E. G.; Gowda, N. M. N.; Reddy, G. K. N. *Polyhedron* **1999**, *18*, 2351.

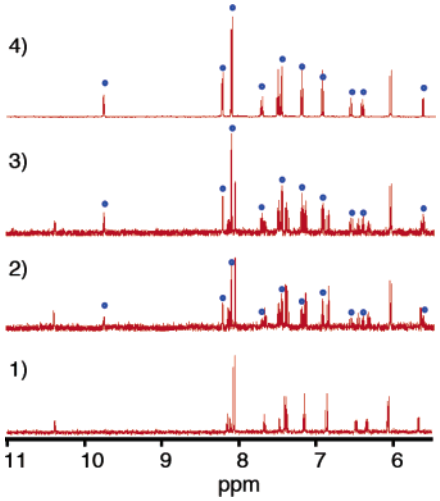

Figure 1. Time-dependent ^{1}H NMR spectra of [Ir(Mebib)(ppy)Cl] in CD_3-CN-d_3. Time after dissolution: (1) 0 h, (2) 17 h, and (3) 62 h. Isolated sample of [Ir(Mebib)(ppy)MeCN](OTf) in CD_3CN-d_3 (4).

Chart 3. Two Possible Geometrical Isomers of [Ir(Mebib)(ppy)Cl]

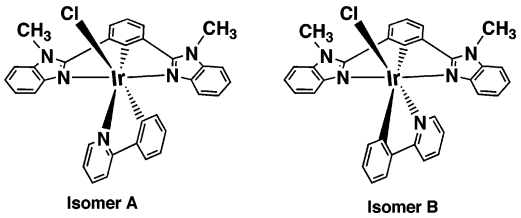

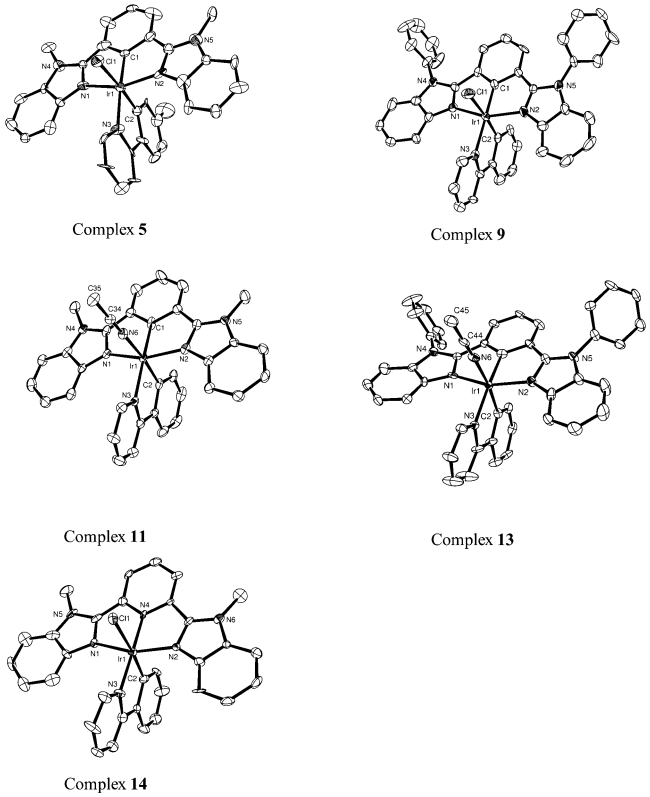

Figure 2. Crystal structures of **5**·$2CH_2Cl_2$, **9**·C_6H_{14}, **11**OTf·Et_2O, **13**OTf, and **14**PF_6·2MeCN·$0.5Et_2O$.

irradiation conditions (6∼12 min irradiation at 650 W) in glycerol, one geometrical isomer was selectively formed. To increase the selectivity, the longer microwave irradiation time and the use of a solvent such as glycerol with a higher boiling point were required for the preparation of [Ir(Mebip)(N∧C)-Cl], compared to that of [Ir(Mebib)(N∧C)Cl]. The pure isomer was obtained by recrystallization from CH_2Cl_2−hexane. Characterization was carefully done by elemental analysis, ^{1}H NMR, and ESI or MALDI-TOF mass spectra. The metathesis reaction of [Ir(Mebib)(N∧C)Cl] with an anionic ligand X (X = Br, I, and CN^-) in ethylene glycol under microwave irradiation gave the corresponding complex [Ir(Mebib)(N∧C)(X)] (X = Br, I, and CN) quantitatively. A ^{1}H NMR chemical shift of the $H_{8'}$ proton on the coordinated ppy of [Ir(Mebib)(ppy)(X)] (X = Cl, Br, I, and CN) around δ 10.2∼10.7 ppm is a good indicator of the anion exchange; that is, the chemical shift reveals the downfield shift in the order X = CN > Cl > Br > I, which is consistent with the increase in the deshielding effect of the Ir−X bond on neighboring $H_{8'}$ protons. The Ir complexes adopt the structure A shown in Chart 3, as confirmed by the X-ray crystallographic analysis described later.

When [Ir(Mebib)(ppy)Cl] was kept in a CD_3CN solution, a new set of ^{1}H signals gradually appeared ($t_{1/2}$ ∼ 20 h; see Figure 1). These new ^{1}H signals are consistent with those of [Ir(Mebib)(ppy)(CH_3CN)](OTf) (**11**), which was separately synthesized and isolated from the substitution reaction of coordinated Cl with CH_3CN in **1**. Furthermore, when the reaction of [Ir(Mebib)(ppy)Cl] (**1**) in CH_3CN was monitored by the absorption spectra, the isosbestic points were observed during the course of the reaction. The time profile of the change in absorbance follows first-order kinetics. In contrast, [Ir(Phbib)(ppy)Cl] (**9**) and [Ir(Mebip)(ppy)Cl]$^+$ (**14**) are less reactive in CD_3CN under the same conditions and the same time domain as those for **1** and show no Cl^- substitution reaction with CD_3CN at room temperature. The sharp contrast for the reactivity difference between **1** and **14** is attributable to the electron richness of **1** compared to **14**. [Ir(R^3bib)(N∧C)Cl] (R^3 = Me or Ph) reacted with Ag(OTf) in CH_3CN to give the cationic complex [Ir(R^3bib)(N∧C)-(CH_3CN)]$^+$ separately. Further, the reaction of [Ir(Mebib)-(ppy)(CH_3CN)]$^+$ (**9**) with phenylacetylene in the presence of potassium fluoride provided a neutral complex, [Ir-(Mebib)(ppy)(CCPh)] (**8**). All of the Ir(III) complexes were characterized by ^{1}H NMR, ESI- and MALDI-TOF MS, and elemental analysis. Single crystals of **5**, **9**, **11**, **13**, and **14** suitable for X-ray crystallographic analysis were obtained by recrystallization from CH_2Cl_2−hexane or CH_3CN−ether, some of which included the solvent.

Crystal Structures of 5·$2CH_2Cl_2$, 9·C_6H_{14}, 11OTf·Et_2O, 13OTf, and 14PF_6·2MeCN·$0.5Et_2O$. The X-ray crystal structures of **5**·$2CH_2Cl_2$, **9**·C_6H_{14}, **11**OTf·Et_2O, **13**OTf, and **14**PF_6·2MeCN·$0.5Et_2O$ are shown in Figure 2. The selected bond distances, bond angles, and torsion angles are provided in Tables 2, 1S, and 2S (1S and 2S as Supporting Information). The coordination geometries of Ir(III) centers for all four complexes were found to be distorted octahedral. The torsion angles are provided in Table 2S, showing that three rings formed by bib tridentate coordination are almost coplanar and that distortion from the planes is relatively small

Table 2. Selected Bond Lengths (Å) for Complexes **5**·2CH_2Cl_2, **9**·C_6H_{14}, **11**OTf·Et_2O, **13**OTf, and **14**PF_6·2MeCN·0.5Et_2O

5		**9**		**11**		**13**		**14**	
Ir(1)−N(1)	2.07(1)	Ir(1)−N(1)	2.058(8)	Ir(1)−N(1)	2.053(4)	Ir(1)−N(1)	2.029(5)	Ir(1)−N(1)	2.037(8)
Ir(1)−N(2)	2.04(1)	Ir(1)−N(2)	2.088(9)	Ir(1)−N(2)	2.050(4)	Ir(1)−N(2)	2.059(5)	Ir(1)−N(2)	2.02(1)
Ir(1)−C(1)	1.92(2)	Ir(1)−C(1)	1.92(1)	Ir(1)−C(1)	1.945(6)	Ir(1)−C(1)	1.965(6)	Ir(1)−N(4)	1.972(7)
Ir(1)−N(3)	2.14(2)	Ir(1)−N(3)	2.15(1)	Ir(1)−N(3)	2.157(4)	Ir(1)−N(3)	2.155(5)	Ir(1)−N(3)	2.059(7)
Ir(1)−C(2)	2.00(1)	Ir(1)−C(2)	1.99(1)	Ir(1)−C(2)	2.013(5)	Ir(1)−C(2)	2.007(6)	Ir(1)−C(2)	2.00(1)
Ir(1)−Cl(1)	2.487(4)	Ir(1)−Cl(1)	2.474(3)	Ir(1)−N(6)	2.113(5)	Ir(1)−N(6)	2.122(5)	Ir(1)−Cl(1)	2.475(3)
				N(6)−C(34)	1.136(7)	N(6)−C(44)	1.138(8)		
				C(34)−C(35)	1.472(8)	C(44)−C(45)	1.468(9)		

Chart 4. Tridentate Pincer Ligand Systems

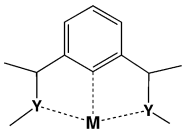

Y = NR_2, PR_2, SR
M = Ir, Rh, Ru, Pd, Pt

except in **4** and **5**. The X-ray structure of **5** reveals that the Ir−C_{bib} bond in the tridentate Ir(Mebib) moiety is located trans to the nitrogen atom in the mppy ligand, while the other Ir−C_{ppy} bond in the Ir(mppy) moiety is trans to the Ir−Cl bond, confirming the structure of the isomers as isomer A in Chart 3. For the structure of **11**, the CH_3CN ligand occupied a trans position in relation to the coordinating carbon atom in ppy, as shown in Figure 2. In four complexes, **5**, **9**, **11**, **13**, two Ir−C bonds were located at the cis position. The cyclometalated Ir−C bonds in the mixed-ligand Ir(bib)(ppy) system induce a strong trans influence on the bond length; that is, the bond lengths of the central Ir−C_{bib} bond are 1.92(2) and 1.945(6) Å for **5** and **9**, while the Ir−N_{ppy} bonds, which are located trans to the Ir−C_{bib} bond, are 2.14(2) and 2.157(4) Å, respectively (Table 2). These Ir−N_{ppy} bond lengths are longer than those of Ir−C_{ppy} [2.00(1) and 2.013(5) Å], which are within the range of typical Ir−C bond lengths. Furthermore, the Ir−Cl bond length at the position trans to the Ir−C_{ppy} bond in **5** [2.487(4) Å] is longer than that seen in $[Ir(tpy)(dmbpy)Cl]^{2+}$ (tpy = 2,2′:6′,2″-terpyridine, dmbpy = 4,4′-dimethyl-2,2′-bipyridine) (2.357 Å).[56] These results indicate that the strong σ donation in the Ir−C bond results in the elongation of Ir−N and Ir−Cl bonds at the trans position. A similar trans influence of Ir−C bonds has been observed in the X-ray crystallographic structures of *fac*- and *mer*-Ir(tppy)$_3$ [tppy = 2-(*p*-tolyl)pyridine].[10] In particular, the Ir−C_{bib} bond lengths are relatively short compared to those of other Ir−C bonds reported in *fac*-Ir(tppy)$_3$ derivatives (average Ir−C = 2.018 Å). The two fused five-membered coordination modes in Ir(N∧C∧N) complexes are relevant to the "pincer"-ligated metal complexes such as [Ir(P∧C∧P)H_2], [Pt(N∧C∧N)Cl], and [Pd(N∧C∧N)l] (see Chart 4), in which the Ir−C bond distances range from 2.00 to 2.09 Å[57,58] and the Pd or Pt−C bond distances are in the range of 1.90∼1.95 Å.[59,60] Further, the Ir−C_{bib} bond length in $[Ir(Mebip)(Mebib)]^{2+}$ was found to be 2.018 Å,[21] which is similar to the values reported for Ir(ppy)$_3$ derivatives. Therefore, the Ir−C_{bib} bond lengths appear to be influenced by not only the steric requirement for the tridentate accommodation of Mebib but also electronic effects. In [Ir(Phbib)(ppy)Cl], the N-phenyl groups adopt a tilted orientation ∼66° to the tridentate Phbib plane (see Table 2S, Supporting Information). In **14**, the Mebip ligand is coordinated to the Ir atom in a tridentate manner, and the Ir−C bond in the Ir−ppy moiety occupies the trans position of the Ir−Cl bond. The Ir−N_{ppy} bond length is 2.059(7) Å. The Ir−Cl and Ir−C_{ppy} bond lengths were found to be 2.475(3) and 2.00(1) Å, respectively, with a trans influence of the Ir−C_{ppy} bonds being observed.

Electrochemistry. Electrochemical data for all of the new Ir(III)−Mebib complexes are summarized in Table 3, together with the UV spectroscopic data. Complex **14** in CH_3CN shows a quasireversible Ir(III/IV) oxidation wave at +1.05 V versus $Fc^{+/0}$ and two reduction waves at −1.52 and −1.91 V versus $Fc^{+/0}$ as reversible and irreversible processes, respectively. Similarly, a reversible Ir(III/IV) oxidation of complex **1** in *N*,*N*′-dimethyl formamide (DMF) occurred at +0.42 V versus $Fc^{+/0}$, while two quasireversible and irreversible reduction processes were observed at −2.42 and −2.80 V versus $Fc^{+/0}$ respectively for Mebib and ppy reductions. The introduction of an Ir−C bond into Ir(N)$_3$(C)$_2$X-type complex **1** induces a large negative shift (∼0.6 V) in the Ir(III/IV) oxidation potential, compared to Ir(N)$_4$(C)X-type complex **14**. The Ir(III/IV) oxidation potential is shifted to the negative direction in the order [Ir(Mebib)(dfppy)CN] (**7**) (+0.77 V) > [Ir(Mebib)(ppy)CN] (**4**) (+0.65 V) > [Ir(Mebib)(dfppy)Cl] (**6**) (+0.57 V) > [Ir(Mebib)(ppy)Cl] (**1**) (+0.42 V) > [Ir(Mebib)(mppy)Cl] (**5**) (+0.40 V), although the first reduction potentials are almost unchanged for all of these complexes (∼−2.40 V vs $Fc^{+/0}$). The substitution of X from Cl to CH_3CN on $[Ir(Mebib)(ppy)X]^{n+}$ induces a large positive shift in the oxidation potential.

UV−vis Absorption Spectra. The UV−vis spectrum of **1** in CH_2Cl_2 shows the MLCT bands at 425, 472, and 523 nm in addition to the $\pi\pi^*$ transition at 244 nm for ppy and 299 and 360 nm for the Mebib ligand (see Figure 3). Upon the substitution of Cl by CN or ppy by dfppy, a shorter wavelength shift of the MLCT band was observed (Figure

(56) Yoshikawa, N.; Sakamoto, J.; Kanehisa, N.; Kai, Y.; Matsumura-Inoue, T.; Takashima, H.; Tsukahara, K. *Acta Crystallogr., Sect. E* **2003**, *59*, m830.
(57) Gottker-Schnetmann, I.; LastName, W. P.; Brookhart, M. *Organometallics* **2004**, *23*, 1766.
(58) Zhang, X.; Emge, T. J.; Ghost, R.; Goldman, A. S. *J. Am. Chem. Soc.* **2005**, *127*, 8250.
(59) Gagliado, M.; Rodriguez, G.; Dam, H. H.; Lutz, M.; Spek, A. L.; Havenith, R. W. A.; Coppo, P.; De Cola, L.; Hartl, F.; van Klink, G. P. M.; van Koten, G. *Inorg. Chem.* **2006**, *45*, 2143.
(60) Williams, J. A. G.; Beeby, A.; Davies, E. S.; Weistein, J. A.; Wilson, C. *Inorg. Chem.* **2003**, *42*, 8609−8611.

Table 3. Absorption Spectral and Electrochemical Data for Ir(Mebib)(R-ppy)X at Room Temperature[a,b]

complex	λ_{abs} nm ($\epsilon \times 10^3/M^{-1}\,cm^{-1}$)	$E_{1/2}^{ox}$ (ΔE_p)[c] or E_{Pa} V vs Fc^+/Fc (mV)	$E_{1/2}^{red}$ (ΔE_p)[c] or E_{Pc} V vs Fc^+/Fc (mV)
[Ir(Mebib)(ppy)Cl] (**1**)	244 (50.0), 299 (38.7), 360 (7.7), 404 (14.0), 425 (15.6), 472(3.1), 523(0.84)	0.42 (60)	−2.46 (66),[d] −2.80[e]
[Ir(Mebib)(ppy)Br] (**2**)	244 (40.0), 300 (29.4), 361 (5.44), 403 (11.4), 424 (12.9), 470sh (2.64), 531 (0.50)	0.46 (60)	−2.45 (68),[d] −2.82[e]
[Ir(Mebib)(ppy)I] (**3**)	250sh (53.5), 267sh (42.4), 299 (38.5), 359 (8.66), 404 (15.1), 423 (15.9), 474sh (3.49),531 (0.88)	0.45 (60)	−2.44 (70),[d] −2.81[e]
[Ir(Mebib)(ppy)CN] (**4**)	242 (54.9), 299 (37.8), 353 (7.9), 392 (15.8), 413 (19.0), 506 (0.35)	0.65 (59)	−2.42 (66),[d] −2.79[e]
[Ir(Mebib)(mppy)Cl] (**5**)	236 (50.0), 300 (44.6), 361 (6.5), 405 (13.5), 426 (15.2), 473 (3.0), 526 (0.75)	0.40 (70)	−2.46 (65),[d] −2.82[e]
[Ir(Mebib)(dfppy)Cl] (**6**)	245 (61.1), 299 (45.6), 355 (8.7), 397 (17.4), 418 (18.7), 455 (3.7), 514 (0.50)	0.57 (60)	−2.40 (65),[d] −2.79[e]
[Ir(Mebib)(dfppy)CN] (**7**)	242 (52.4), 298 (35.0), 349 (7.7), 386 (15.2), 407 (17.6), 498 (0.30)	0.77 (58)	−2.37 (66),[d] −2.70[e]
[Ir(Mebib)(mppy)(CCPh)] (**8**)	236 (68.3), 272(56.2), 298 (63.7), 360 (6.9), 419 (12.9), 437 (15.9), 482 (3.4), 530 (0.88)	0.61 (65)	−2.49 (65),[d] −2.90[e]
[Ir(Phbib)(ppy)Cl] (**9**)	301 (39.3), 406 (15.3), 429 (17.1), 527 (0.52)	0.52 (60)	−2.36 (68),[d] −2.78[e]
[Ir(Phbib)(ppy)CN] (**10**)	298 (43.0), 393 (18.1), 414 (21.5), 510 (0.38)	0.78 (60)	−2.24 (60),[d] −2.69[e]
$[Ir(Mebib)(ppy)(MeCN)]^+$ (**11**)[b]	247 (50.5), 298 (37.2), 380 (17.9), 398 (18.2), 496 (0.36)	0.81 (65)	−2.32,[e] −2.57,[e] −2.75[e]
$[Ir(Mebib)(mppy)(MeCN)]^+$ (**12**)	245 (65.4), 296 (50.1), 379 (22.2), 396 (23.1), 490 (0.27)	*f*	*f*
$[Ir(Phbib)(ppy)(MeCN)]^+$ (**13**)	245sh (64.9), 297 (32.8), 381 (17.3), 400 (17.4), 498 (0.61)	*f*	*f*
$[Ir(Mebip)(ppy)Cl](PF_6)$ (**14**)	242 (38.2), 313 (27.2), 348 (23.9), 510 (0.42), 575 (0.14)	1.05[e]	−1.52 (68),[d] −1.91[e]

[a] UV−vis spectra were measured in CH_2Cl_2 and electrochemical data in DMF unless otherwise noted. [b] Electrochemical measurement was done in CH_3CN. [c] Peak-to-peak separation. [d] Quasireversible process. [e] Irreversible process. [f] Not measured.

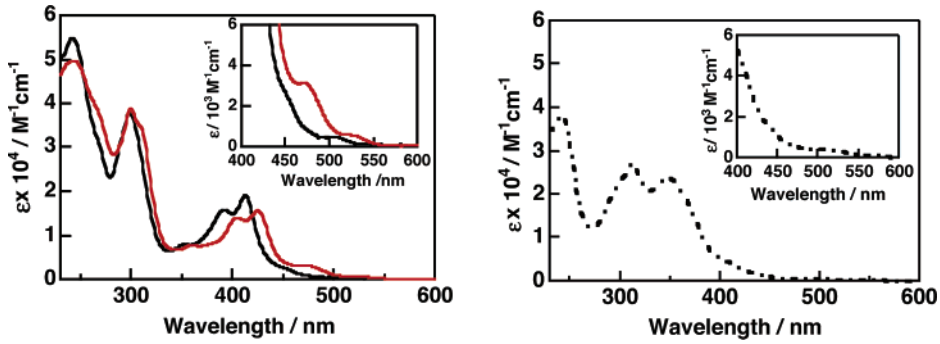

Figure 3. UV spectra of Ir complexes **1** (red) and **4** (black) in CH_2Cl_2 and **14** (black, dashed line) in CH_3CN at room temperature.

3). In contrast, the UV absorption maxima of [Ir(Mebip)(ppy)X] are unaltered by the substitution of X = Cl to Br or I, which is unexpected. Further, the alternation of methyl to a phenyl group on the benzimidazole moiety leads to a slightly longer wavelength shift on the MLCT band, while the spectral shapes are almost identical. The band around 510∼530 nm can be assigned as a triplet MLCT band, compared to other reported Ir(ppy) complexes. This MLCT band for [Ir(Mebib)(R-ppy)X] is shifted to a shorter wavelength in the order **5** > **1** > **6** > **4** > **7**, and at the same time, the intensity of the band is decreasing in this order (Table 3).

Emission Spectra. Figure 4 shows the emission spectra of **1** in Ar-saturated CH_2Cl_2 at 295 K and CH_2Cl_2−toluene (1:1 v/v) at 77 K. The complex exhibits a strong emission band with a vibrational structure at around 555 nm with a lifetime of 1.20 μs at room temperature. In a glass matrix at 77 K, the emission spectra of all of the Ir(III)−Mebib and Ir(III)−Phbib complexes exhibited almost the same vibrational structures with a small sideband at about 1500 cm^{-1} lower, while for the Ir−Mebip complex **14**, a vibrational sideband appeared approximately 1360 cm^{-1} lower with a relatively high intensity. Emission maxima of **1** were tuned by the substitution of ppy or Cl; that is, the maxima were shifted to a shorter wavelength in the order **1** ∼ **5** > **6** > **4** > **7** (Figure 5 and Table 4). A strong relationship between UV spectral data and electrochemical data has been reported.[61] In the Ir−Mebib complexes, plots of emission maxima versus the redox potential are shown in Figure 6. The Ir(III/IV) oxidation potential shows a good linear relationship with the emission maxima; in contrast, the reduction potential appears to remain almost constant upon changes in the emission maxima. This linear relationship strongly indicates that the excited state of [Ir(L)(N∧C)X] complexes has considerable MLCT character.

The emission maxima of the Ir complexes shift to higher energy (600∼675 cm^{-1}) on going from room temperature to 77 K. A relatively large rigidochromic shift indicates a

(61) Vlcek, A. A.; Dodsworth, E. S.; Pietro, W. J.; Lever, A. B. P. *Inorg. Chem.* **1995**, *34*, 1906 and references therein.

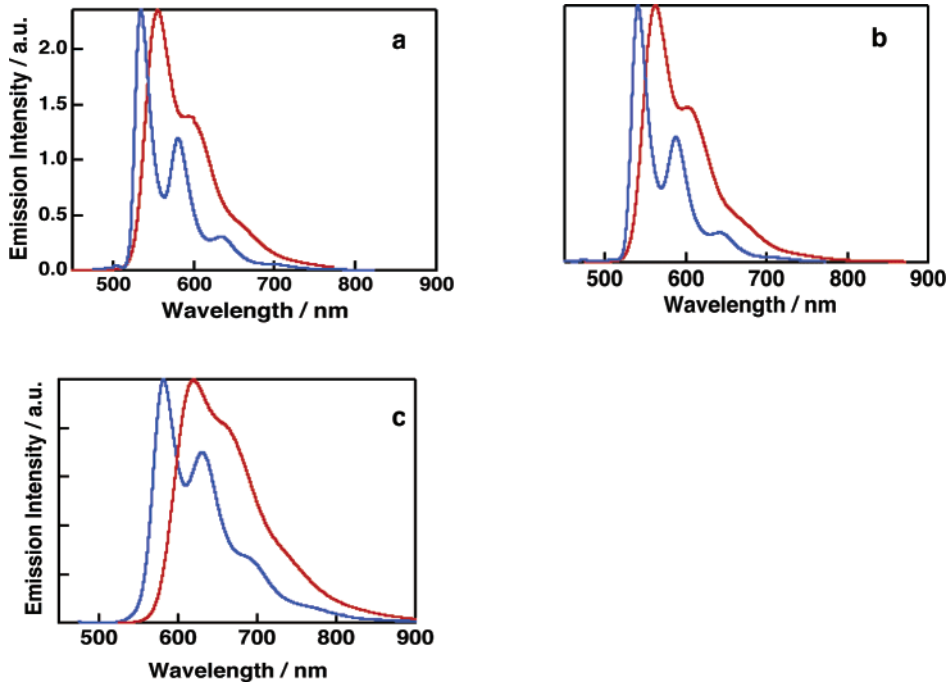

Figure 4. Emission spectra of complexes **1** (a) and **9** (b) in Ar-saturated CH_2Cl_2 at room temperature (red) and in CH_2Cl_2−toluene (1:1 v/v) (red) at 77 K (blue) and **14** (c) in Ar-saturated CH_3CN at room temperature (red) and in DMF−EtOH−MeOH (1:5:5 v/v) at 77 K (blue).

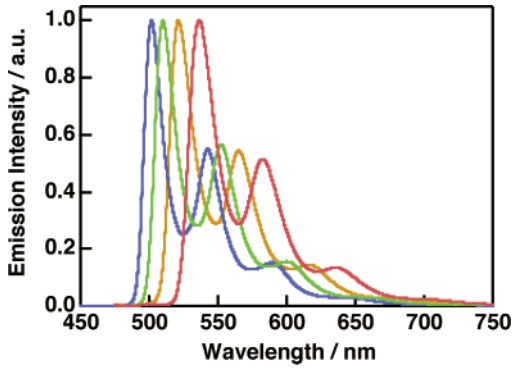

Figure 5. Emission spectra of Ir complexes **7** (blue line), **4** (green), **6** (orange), and **1** (red) in CH_2Cl_2−toluene (1:1 v/v) at 77 K.

greater polarity of the excited state. A similar rigidochromic effect has been previously reported for $[Ir(ppy)_3]$ derivatives and emissive metal complexes.[9,62] Surprisingly, all of the present neutral Ir(III) complexes [Ir(L)(R-ppy)X] (L = Mebib and Phbib; R = H, CH_3, and F; X = Cl and CN) exhibited a high luminescent quantum yield (Φ = 0.63∼0.95), with [Ir(Phbib)(ppy)Cl] having the highest yield of Φ = 0.95. Several Ir complexes containing bidentate ppy derivatives have been reported to have high quantum yields; for example, $[Ir(tppy)_3]$ and $[Ir(ppbi)_2(acac)]$ have luminescent quantum yields of 0.54 and 0.78, respectively.[3,10] However, variations in the substituent of ppy leads to large changes in the quantum yield. In the present system, the luminescent quantum yields were high even if the substituent of ppy was changed. The values of the radiative rate constant (k_r) for the [Ir(Mebib)(R-ppy)X] complexes range from 3.9×10^5 s^{-1} for [Ir(Mebib)(ppy)CN] to 5.5×10^5 s^{-1} for [Ir(Mebib)-(mppy)Cl], while those of the nonradiative rate constant (k_{nr}) are from 0.6×10^5 s^{-1} for [Ir(Mebib)(dfppy)CN] to 1.6×10^5 s^{-1} for [Ir(Mebib)(mppy)Cl]. The k_r values are greater than those reported for $[Ir(ppy)_3]$ (2.0×10^5 s^{-1}) and $[Ir-(ppy)_2(acac)]$ (2.1×10^5 s^{-1}). The substitution of the ligand L from Mebip to Mebib in [Ir(L)(ppy)Cl] leads to a shorter wavelength shift of emission maxima and an increasing quantum yield. On the other hand, the emission maxima of [Ir(Mebib)(ppy)X] are unaltered by the substitution of X= Cl to Br or I, which is reflected in the UV absorption spectra. As for the complexes $[Ir(Mebib)(ppy)(CH_3CN)]^+$ and $[Ir-(Mebib)(mppy)(CH_3CN)]^+$, the substitution of Cl with CH_3-CN leads to a drastic decrease in the luminescent quantum yield (Φ = 0.24 and 0.22, see Table 4), while a high quantum yield is maintained for the complex [Ir(Mebib)(mppy)-(CCPh)] prepared by the replacement of Cl in the complex. Plots of k_r and ln k_{nr} values versus emission energy are shown in Figures 7a and b. Although radiation theory predicts that the k_r value is proportional to the cube of the emission energy,[63] the k_r values of these Ir complexes fall as the emission energy increases (Figure 7a). However, employing Mebip instead of Mebib leads to a decrease in the emission energy, and the k_r values decrease considerably. The variations in the radiative rate with tridentate ligands or X are relevant to the phosphorescence mechanism of these Ir complexes, and evaluations of k_r values based on DFT calculations are described later.

On the basis of the linear relationship of ln k_{nr} versus the emission energy (Figure 7b), the present Ir system closely

(62) Cummings, S. D.; Eisenberg, R. *J. Am. Chem. Soc.* **1996**, *118*, 1949−1960.

(63) Strickler, S. J.; Berg, R. A. *J. Chem. Phys.* **1962**, *37*, 814.

Table 4. Photophysical Properties of [Ir(Mebib)(Rppy)X] in Ar-Saturated CH_2Cl_2

complex	λ_{em}/nm		S_M, ν/cm^{-1}	τ/ms		Φ^a	k_r	k_{nr}
	295 K	77 K[b]	77 K	295 K	77 K[b]		10^5 s^{-1}	10^5 s^{-1}
[Ir(Mebib)(ppy)Cl](**1**)	555	535, 580, 633	0.85, 1490	1.78 (1.61)[c]	2.22 (2.84)[c]	0.78 (0.59)[c]	4.4 ± 0.30 (3.7 ± 0.35)[c]	1.2 ± 0.30 (2.6 ± 0.35)[c]
[Ir(Mebib)(ppy)Br](**2**)	553	532, 579, 632	0.78, 1490	1.73	2.28	0.87	5.0 ± 0.26	0.8 ± 0.26
[Ir(Mebib)(ppy)I](**3**)	553	533, 579, 632	0.76, 1480	1.83	2.28	0.81	4.4 ± 0.25	1.0 ± 0.25
[Ir(Mebib)(ppy)CN](**4**)	526	510,552,600	0.84, 1510	2.17	2.50	0.84	3.9 ± 0.26	0.7 ± 0.26
[Ir(Mebib)(mppy)Cl](**5**)	556	536,582,636	0.77, 1490	1.40	2.28	0.77	5.5 ± 0.36	1.6 ± 0.36
[Ir(Mebib)(dfppy)Cl] (**6**)	540	521, 565,616	0.82, 1480	1.63	2.26	0.86	5.3 ± 0.33	0.9 ± 0.33
[Ir(Mebib)(dfppy)CN] (**7**)	517	501, 542, 590	0.82, 1490	2.50	2.70	0.85	3.4 ± 0.20	0.6 ± 0.20
[Ir(Mebib)(mppy)(CCPh)] (**8**)	563	542, 590, 645	0.74, 1520	1.46	2.33	0.75	5.1 ± 0.30	1.7 ± 0.30
[Ir(Phbib)(ppy)Cl] (**9**)	562	541, 588, 645	0.74, 1490	1.55	2.17	0.95	6.1 ± 0.29	0.3 ± 0.29
[Ir(Phbib)(ppy)CN](**10**)	533	515, 558, 608	0.80, 1490	2.02	2.45	0.89	4.4 ± 0.24	0.5 ± 0.24
[Ir(Mebib)(ppy)(MeCN)]$^+$ (**11**)	513	520, 564, 614	0.83, 1510	0.96	2.82	0.24	2.5 ± 0.52	7.9 ± 0.52
[Ir(Mebib)(mppy)(MeCN)]$^+$ (**12**)	512	519, 562, 614	0.85, 1500	0.79	2.86	0.22	2.9 ± 0.75	9.9 ± 0.75
[Ir(Mebip)(ppy)Cl](PF_6) (**14**)	610	578	1.05, 1360	2.00	13.5	0.16	0.80 ± 0.25	4.20 ± 0.25

[a] The emission quantum yields of the Ir(III) compounds were determined using DPA (= 0.91)[24] as a reference. The error in the yields is ±5%. [b] In CH_2Cl_2−toluene (1:1 v/v). [c] In Ar-saturated CH_3CN.

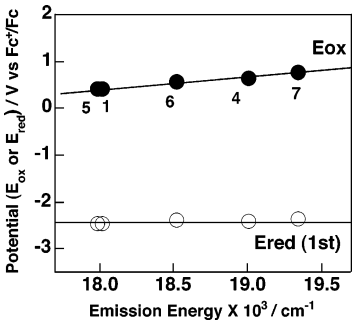

Figure 6. Plots of emission energies vs redox potentials (the number in the plots corresponds to the complex numbering).

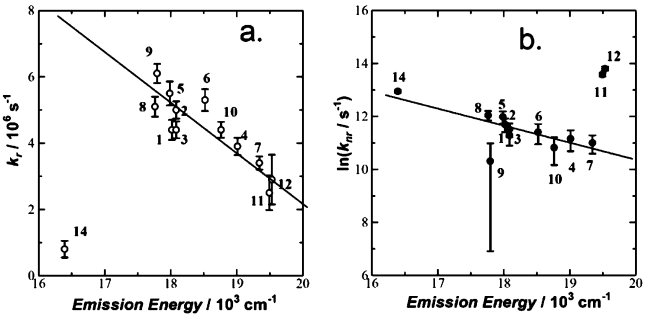

Figure 7. Plots of k_r values vs emission energy (a) and plots of ln k_{nr} vs emission energy (b).

follows the energy gap law,[64] except for X = CH_3CN. The Ir complexes with CH_3CN show somewhat shorter lifetimes at room temperature, while the lifetimes at 77 K are comparable to those of the other Ir−Mebib complexes, suggesting the presence of additional decay pathways involving thermally accessible excited states such as via ^{3}dd.

DFT Calculations. To shed light on the characterization of the emitting states in the present iridium complexes, DFT calculations were carried out for the Ir complexes with available X-ray structures. Frontier molecular orbitals (MOs) of complex **5** obtained at the B3PW91/LAN2DZ level are shown in Figure 8. For complex **5**, both the highest occupied molecular orbital (HOMO) and HOMO-1 are formed from a combination of Ir 5d and Cl 2p orbitals in an antibonding

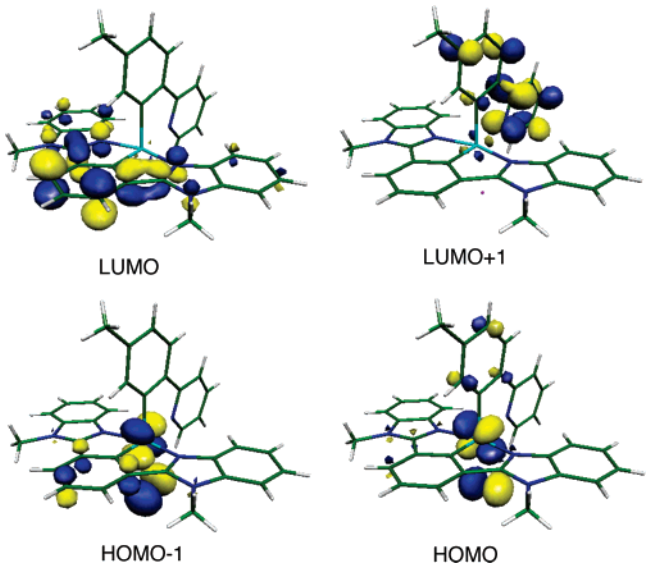

Figure 8. Frontier molecular orbitals of complex **5**, which were obtained by DFT calculation at the B3PW91/LANL2DZ level.

fashion, while the lowest unoccupied molecular orbital (LUMO) and LUMO+1 originate from Mebib π^* and ppy π^* orbitals, respectively.

The energy differences between the HOMOs and occupied orbitals with a larger contribution of Ir 5d are one of the important factors determining the k_r values of phosphorescence.[65,66] Orbital energy levels for complexes **5**, **11**, and **14** are depicted in Figure 9 together with their orbital parentage. The differences in orbital energy between HOMO and HOMO-1 are 0.20 eV for **5**, 0.33 eV for **11**, and 0.50 eV for **14**, reflecting orbital interactions with the ligands. The Ir d_{xy} orbital in these Ir complexes is the most destabilized among the Ir t_{2g} orbitals because of π donation from both a phenyl anion in ppy and imidazole moieties in Mebib or Mebip and thus contributes to the HOMO. HOMO-1 of these Ir complexes is composed of the Ir d_{yz} orbital, which is destabilized by mixing with π orbitals of a

(64) Kober, E. M.; Caspar, J. V.; Lumpkin, R. S.; Meyer, T. J. *J. Phys. Chem.* **1986**, *90*, 3722.
(65) Siddique, Z. A.; Yamamoto, Y.; Ohno, T.; Nozaki, K. *Inorg. Chem.* **2003**, *42*, 6366.
(66) Siddique, Z. A.; Ohno, T.; Nozaki, K.; Tsubomura, T. *Inorg. Chem.* **2004**, *43*, 663.

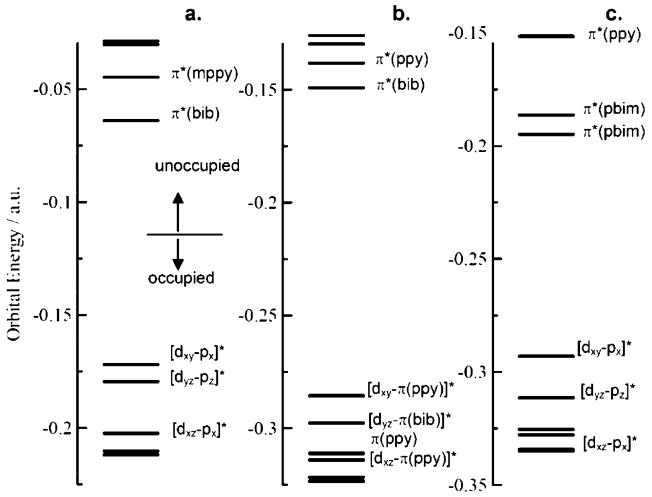

Figure 9. MO levels calculated at the B3PW91/LANL2DZ level for X-ray structures of [Ir(Mebib)(mppy)Cl] (**5**) (a), $[Ir(Mebib)(ppy)CH_3CN]^+$ (**11**) (b), and $[Ir(Mebip)(ppy)Cl]^+$ (**14**) (c). The molecule is oriented so that the *z* axis is the C_2 axis of the tridentate ligand and the *y* axis is parallel with the Ir−X bonding.

phenyl moiety in Mebib involving **5** and **11** or the pyridyl moiety in Mebip of **14**; however, the Ir d_{yz} orbital of **14** is less destabilized because of the weaker π-donating ability of Mebip, and thus, the energy difference between HOMO and HOMO-1 is much larger than in the Ir−Mebib complexes. As shown in Figure 9, the energy gap in **5** is smaller than that for **11** because Ir d_{xy} and d_{yz} orbitals are considerably destabilized by the antibonding interaction with the Cl $2p_x$ and $2p_z$ orbitals, respectively.

The LUMO of these Ir−Mebib complexes is the π^* orbitals of Mebib, which is consistent with the observed invariance of the first reduction potentials in the Ir−Mebib complexes. Further, the π^* orbitals of ppy are located at a higher energy than those of Mebib. For complex **14**, the LUMO and LUMO+1 are localized on the 2-pyridylbenzimidazolyl moiety (pbim) in Mebip, which is probably due to the deconstructive interaction between the π^* orbitals of two pbim moieties through the phenylene group. Consequently, the promoted electron in MLCT states of Ir−Mebip complexes is not delocalized over the Mebip ligand but instead tends to be localized on one of the pbim moieties, which is probably responsible for the pronounced vibrational sideband in the emission spectra of complex **14** (Figure 4c).

Time-dependent DFT calculations revealed that the electronic configuration of the lowest triplet MLCT state involves primarily the HOMO and LUMO (Tables 3S, 4S, and 5S in the Supporting Information), and therefore, the emitting state consists of the combination of Ir dπ to Mebib π^* ligand charge transfer (MLCT) and Cl 3p to Mebib π^* (XLCT) in the Ir complexes with the Cl anion. In particular, the orbital mixing in an antibonding fashion between Ir dπ and Cl 2p orbitals plays an important role in controlling the MLCT characters in these complexes, which can determine the excited-state properties such as radiative and nonradiative rate constants and quantum yields. Concerning the complex having CH_3CN as X, the lowest state is characterized by a mixture of MLCT and $\pi\pi^*$ of the ppy and Mebip ligands. The replacement of Cl by CH_3CN with weak π-donating ability does not give remarkable change in k_r, as shown in Table 3.

Mechanism of High Phosphorescence Yield in [Ir(Mebib)(ppy)Cl]. The phosphorescence of transition metal complexes originates from the mixing of emissive singlet states into the lowest triplet state due to spin−orbit coupling of the d electrons. The transition dipole moments of the singlet states are therefore the origin of the radiative capability of the lowest triplet state. The radiative rate constant k_r of phosphorescence can be calculated from the transition dipole moment of the perturbed triplet state using the following expression:

$$k_r = \frac{16\pi^3 \times 10^6 E^3 n^3}{3h\epsilon_0}|M|^2 \qquad (1)$$

where E is the emission energy and n, h, and ϵ_o are the refractive index of the medium, Planck's constant, and the vacuum permittivity, respectively. According to the first-order perturbation theory, the transition dipole moment from the triplet state to the ground state M_T is given by

$$M_T = \sum_n \frac{\langle \Psi_T | H_{SO} | \Psi_{Sn} \rangle}{{}^3E_T - {}^1E_{S_n}} M_{Sn} \qquad (2)$$

where Ψs and Es are eigenfunctions and eigenvalues of the Hamiltonian without spin−orbit coupling (H_{SO}), respectively. M_{S_n} is the transition dipole moment from the nth singlet state to the ground state. Thus, the radiative rate constant of the phosphorescence is dominated by three factors: spin−orbit coupling matrix element, the energy gap between T_1 and S_n, and Ms.

The radiative rate of ${}^3\pi\pi^*$ in Rh(III) compounds has been proposed to be the result of two entirely different mechanisms.[67−69] In one mechanism, the increase in the radiative character induced by heavy metal is ascribed to a direct spin−orbit coupling between ${}^3\pi\pi^*$ and ${}^1d\pi^*$ (= ^{1}MLCT) electronic configurations.[67] This hypothesized mechanism, however, does have drawbacks. Because the spin−orbit coupling between ${}^3\pi\pi^*$ and ${}^1d\pi^*$ involves only the two-center integrals on the metal center, the magnitudes of the spin−orbit coupling are usually quite small. Therefore, the spin−orbit coupling between ${}^3\pi\pi^*$ and ${}^1d\pi^*$ does not seem to be responsible for the large effect of the heavy metal. Accordingly, Miki et al. have proposed a new mechanism in which ${}^3\pi\pi^*$ is mixed with ${}^3d\pi^*$ by a configurational interaction because the mixing between ${}^3d\pi^*$ and ${}^1d\pi^*$ is induced effectively by one-center spin−orbit coupling.[68,69] Thus, the magnitude of the spin−orbit coupling element in eq 2 increases as the contribution of the ${}^3d\pi^*$ electronic configuration in the lowest triplet state increases. In an

(67) Komada, Y.; Yamauchi, S.; Hirota, N. *J. Phys. Chem.* **1986**, *90*, 6425.
(68) Miki, H.; Shimada, M.; Azumi, T.; Brozik, J. A.; Crosby, G. A. *J. Phys. Chem.* **1993**, *97*, 11175.
(69) (a) Azumi, T.; Miki, H. *Top. Curr. Chem.* **1997**, *191*, 1. (b) Solomon, E. I.; Lever, A. B. P. *Inorganic Electronic Structure and Spectroscopy*; John Wiley & Sons: New York, 1999; Vol. I, Chapter 1.

Table 5. Data Used for the Evaluation of Phosphorescence Radiative Rate Constants

	Ir(Mebib)(mppy)Cl (**5**)	$[Ir(Mebib)(ppy)CH_3CN]^+$ (**11**)	$[Ir(Mebip)(ppy)Cl^+$ (**14**)
		T_1	
E/eV[a]	1.97	2.62	1.72
C_{dxy}[b]	0.63	0.58	0.56
		S_n	
E/eV[a]	2.49 (S_2)	3.43 (S_3)	2.50 (S_3)
C_{dyz}[b]	0.58	0.48	0.44
f[a]	0.074	0.227	0.024
ΔE (S_n-T_1)/ cm^{-1}	4190	6530	6290
SOC (S_n-T_1)/cm^{-1} [c]	809	617	546
k_r/s^{-1} ($n = 1.42$)[d]	1.0×10^6	1.3×10^6	4.6×10^4
$k_{r,obsd}/s^{-1}$ (CH_2Cl_2)	4.4×10^5	2.5×10^5	8.0×10^4

[a] Obtained from the calculation at the TD-B3PW91/LANL2DZ level. [b] Coefficient of the natural atomic orbital of Ir 5d in HOMO (T_1) or HOMO-1 (S_n) obtained from NBO analysis. [c] Absolute value of the spin−orbit coupling matrix element calculated from eq 4. [d] Value calculated using eq 3.

alternative interpretation using recent MO theory, the electronic state is often described by a linear combination of electronic transitions between delocalized MOs constructed by a combination between metal-centered and ligand-centered orbitals. Using the MO model, the coupling element in eq 2 increases with the increase in the contribution of d orbitals in the MOs ascribed to the lowest triplet state. Because the DFT calculation for the present Ir complexes indicates a greater contribution of the Ir 5d orbital in the HOMO, as shown in Figures 8 and 9, one-center spin−orbit coupling between $^3d\pi^*$ and $^1d\pi^*$ is considered to be the predominant mechanism for the intense phosphorescence of the complexes.

Theoretical consideration of spin−orbit coupling places further restrictions on the electronic configuration of $^1d\pi^*$, which can be coupled with $^3d\pi^*$ in the lowest triplet state.[65,66,70] Both $^3d\pi^*$ and $^1d\pi^*$ should involve the same π^* orbital because spin−orbit couplings of π electrons are negligibly small. Furthermore, as any atomic angular momenta in low-symmetry transition metal complexes are quenched, the spin−orbit coupling of the d electron works between the $d\pi^*$ configurations involving different d orbitals. Consequently, under the assumption of one-center spin−orbit integrals, the $^3d\pi^*$ electronic configuration in the lowest state is effectively coupled with the specific $^1d\pi^*$ configurations involving the d orbital with a different orientation and having a common π^* orbital.[65,66,70]

The temperature-dependent density functional theory (TD-DFT) calculation of complex **5** at the B3PW91/LANL2DZ level indicates that the lowest triplet state (T_1) is the HOMO → LUMO electronic configuration in which the donor $5d_{xy}$ orbital interacts with the accepting Mebib π^* in a pseudo-δ bonding fashion. As described above, spin−orbit coupling of the Ir 5d electron effectively mixes $5d_{xy}$ → LUMO in T_1 with the other MLCTs from different d orbitals to LUMO. Thus, T_1 is mixed with $5d_{yz}$ → LUMO in S_2 and $5d_{xz}$ → LUMO in S_6 (see Figure 9 and Table 3S). Because the oscillator strengths (f) of S_2 and S_6 are 0.074 and 0.009, respectively, the intense phosphorescence of complex **5** originates from the mixing between S_2 and T_1 because of the spin−orbit coupling of Ir 5d electrons. This phosphorescence mechanism is then confirmed by evaluating the k_r value using a crude approximation of the one-center spin−orbit coupling element. From the definition of oscillator strength in vacuo $f = 8\pi^2 mE|M|^2/3he^2$ and eq 2, eq 1 can be transformed as

$$k_r(T_1) \approx \frac{n^3 E_T^{\ 3}}{1.5}\left(\frac{\langle S|H_{SO}|T\rangle}{E_S - E_T}\right)^2 \times \frac{f_S}{E_S} \qquad (3)$$

where the emission energy E and matrix element are in cm^{-1}. Among the spin−orbit coupling elements between S_2 ($d_{yz} \rightarrow \pi^*$) and triplet sublevels of T_1 ($d_{xy} \rightarrow \pi^*$), that is, $T_{1,x}$, $T_{1,y}$, and $T_{1,z}$, only the element involving $T_{1,y}$ has a nonzero value. When the element between spin−orbitals involving ζ ($= d_{xy}$) and ξ ($= d_{yz}$) given in eq 9 in ref 69a or eq 67 in ref 69b, the one-center spin−orbit coupling element can be evaluated as

$$\langle S_2|H_{SO}|T_{1,y}\rangle = \frac{i}{2}(\langle C_{dxy}d_{xy}^{\alpha}|H_{SO}|C_{dyz}d_{yz}^{\beta}\rangle - \langle C_{dxy}d_{xy}^{\beta}|H_{SO}|C_{dyz}d_{yz}^{\alpha}\rangle) = \frac{i}{2}\zeta_{Ir-5d}C_{dxy}C_{dyz} \qquad (4)$$

where ζ_{Ir-5d} is the one-electron spin−orbit coupling constant of the 5d electron in iridium and C_{dxy} and C_{dxz} are the coefficients of the 5d orbital involved in HOMO and HOMO-1, respectively. Using theoretical values of $\zeta_{5d-Ir} = 4430$ cm^{-1} for the Ir(III) ion,[70,71] ΔE (S_2-T_1) = 4190 cm^{-1}, and $f = 0.074$ obtained by TDDFT and the coefficients of natural atomic orbitals obtained using an NBO 5.0 program[72] of $C_{dxy} = 0.63$, $C_{dxz} = 0.58$, and $n = 1.42$ (CH_2Cl_2), eq 3 gives 1.0×10^6 s^{-1} as the k_r value of complex **5**. For complex **11**, a similar analysis indicates that spin−orbit coupling with S_3 is the origin of the radiative probability of the T_1 state, and the k_r value is calculated as 1.3×10^6 s^{-1} (Table 5).

A rather smaller k_r value of 4.6×10^4 s^{-1} is predicted for the Ir−Mebip complex **14**. Thus, it turns out that the evaluation based on one-center spin−orbit coupling almost reproduces the magnitude of k_r values of the present Ir

(70) Nozaki, K. *J. Chin. Chem. Soc.* **2006**, *53*, 101.

(71) Fraga, S.; Saxena, K. M. S.; Karwowski, J. *Handbook of Atomic Data. Physical Sciences Data*; Elsevier: Amsterdam, The Netherlands, 1976; Vol. 5.

(72) Weinhold, F.; Landis, C. R. *Chem. Ed.: Res. Practice Eur.* **2001**, *2*, 91.

complexes. The relatively large deviation for complex **11** can be ascribed to the oversimplifications of spin−orbit interactions: a more reliable evaluation would require the consideration of spin−orbit interactions with many excited states and geometrical changes of emitting states.[70] Nevertheless, the present simplified analysis can rationalize the observed variation of k_r values. As shown in Table 4, the replacement of Cl by CH_3CN does not cause a large change in k_r. HOMO-1 in the Cl complex **5** is composed of Ir 5d and Cl 3p orbitals, while HOMO-1 in the CH_3CN complex **11** is produced from Ir 5d and Mebib π orbitals. The larger contribution of Mebib π orbitals in HOMO-1 in complex **11** gives rise to the stronger oscillator strength of S_3 (HOMO-1 → LUMO) from which the T_1 state borrows its intensity. On the other hand, the larger contribution of Mebib orbitals in HOMO-1 increases the magnitude of the exchange integral in S_3 and thereby increases the energy gap $\Delta E(S_3-T_1)$, which compensates for the increase in the oscillator strength of S_3. Consequently, the resulting k_r value of phosphorescence is almost the same as that of complex **5**.

In the Mebip complex (**14**), because the LUMO is localized on the pbim moiety, as described above, it mixes only weakly with HOMO-1 with C_s symmetry, which is responsible for the rather small oscillator strength of S_3 (HOMO-1 → LUMO). Moreover, the energy gap $\Delta E(S_3-T_1)$ is larger than that for complex **5** because of a larger energy difference between HOMO and HOMO-1 (Figure 9). Both of these effects remarkably reduce the k_r value of phosphorescence in the Mebip complex.

The TDDFT calculation indicates that the transition dipole moments of S_2 in **5** and S_3 in **11** are oriented along the x axis, not along the CT direction, that is, the C_2 axis of the Ir−Mebib subunit. The origin of the transition dipole moment of MLCT in a mononuclear complex has been studied by Day and Sanders.[73] When a transition metal ion is coordinated to ligands, the d orbitals interact with the π^* orbitals to form the donor and acceptor orbitals ascribed to CT transitions. Mixing of the other metal-centered or ligand-centered orbitals will lead to other sources of intensity. The donor and the acceptor orbitals ascribed to the CT transition are then given by

$$\phi_D = \phi_d + \lambda_a\phi_{\pi^*} + \lambda_b\phi_\pi + \lambda_c\phi_{\pi'^*}$$
$$\phi_A = \phi_{\pi^*} - \lambda_a\phi_d + \lambda_f\phi_p + \lambda_g\phi_{p^*} \quad (5)$$

where ϕ_d and ϕ_p are the metal-centered d and p orbitals, respectively, and π and π'^* are ligand-centered occupied or unoccupied orbitals, respectively, other than π^*. λ is the mixing coefficient. The mixing coefficients increase with increasing resonance integrals between orbitals. Normalization factors are neglected for simplification. Ignoring higher-order terms, the transition dipole moment (M) of the CT transition is thus given by

$$M_{CT} = \langle\phi_d|\mu|\phi_{\pi^*}\rangle + \lambda_a(\langle\phi_{\pi^*}|\mu|\phi_{\pi^*}\rangle - \langle\phi_d|\mu|\phi_d\rangle) + \lambda_b\langle\phi_\pi|\mu|\phi_{\pi^*}\rangle + \lambda_c\langle\phi_{\pi'^*}|\mu|\phi_{\pi^*}\rangle + \lambda_f\langle\phi_d|\mu\phi_p\rangle + \lambda_g\langle\phi_d|\mu|\phi_{p^*}\rangle \quad (6)$$

where μ denotes a dipole operator. The first term is the contact CT term, which is usually negligible. The second is the product of a mixing coefficient and the dipole moment of the transferred charge, often called the transfer term. The transfer term should be the origin of the intensity of the MLCT transitions between the d and π^* orbitals with a large resonance integral, and therefore, the transition dipole moment is oriented along the CT direction. The intense MLCT absorption in tris(2,2′-bipyridine) complexes of Fe(II), Ru(II), and Os(II) with a D_3 point group is ascribed to the transfer term in e → e transitions.[74−76] Recent theoretical investigation of the phosphorescence in [*fac*-Ir(ppy)$_3$] and $[Ru(bpy)_3]^{2+}$ has revealed that the lowest triplet state borrows the transfer term of the $^1d\pi^*$ ($b_1 \rightarrow b_1$) transition in the pseudo-C_{2v} point group.[70]

The other four terms in eq 6 are the moments borrowed from interunit transitions. The third term is the moment borrowed from $^1\pi\pi^*$ due to d-orbital delocalization over the ligands. The fourth term is borrowed from the transition between π^* and π'^*. The latter is the unoccupied orbital mixed into the d orbital through π back-donation. The fifth and sixth terms are the moments of Laporte-allowed metal-centered transition d ↔ p. The intensity-borrowing mechanism could possibly contribute to the CT intensity when the resonance integral between d and π^* is very small because of their unfavorable overlapping. In particular, when the d and π^* orbitals interact in a π-bonding fashion but are different in symmetry, the d orbital is mixed with π and π'^*, for which the symmetry is different from that of the accepting π^* orbital. In such complexes, the CT band may borrow intensity from the $\pi \rightarrow \pi^*$ transition or from the transition between unoccupied ligand orbitals $\pi'^* \leftrightarrow \pi^*$. The intensity of the e → a_2 transition in $[Ru(bpy)_3]^{2+}$ with the D_3 point group is considered to borrow from the transition between unoccupied ligand orbitals e → a_2.[76]

The contributions of parent fragment orbitals in each frontier MO of Ir(Mebib)(mppy)Cl (**5**) were calculated using the ADF program package and are summarized in Table 6. Because the contributions were calculated at the pure DFT level, they are somewhat different from those determined by the hybrid B3PW91 calculations shown in Figure 9 and Table 5; in particular, the contributions of Cl 3p in HOMO and HOMO-1 seem to be rather large compared with those at the hybrid DFT level. The HOMO is characterized primarily by antibonding between Cl $3p_x$ and Ir $5d_{xy}$, with a small contribution of the occupied 31st MO in mppy (ppy-31) and the 61st MO in Mebib (bib-61) and of the unoccupied 64th MO in Mebib (bib-64*). The HOMO-1 is antibonding between Cl $3p_z$ and Ir $5d_{yz}$ with small contributions of bib-62, bib-65*, and bib-68*. While the LUMO is formed from bib-64*, the LUMO+1 is from ppy-33*. The transition dipole moment of the CT transition GS ↔ S_2 cannot be accounted for by the transfer term because the donor d_{yz} and the acceptor bib-64* orbital are different in

(73) Day, P.; Sanders, N. *J. Chem. Soc. A* **1967**, 1530.
(74) Daul, C.; Schlaepfer, W. *J. Chem. Soc., Dalton Trans.* **1988**, 393.
(75) Kober, E. M.; Meyer, T. J. *Inorg. Chem.* **1982**, *21*, 3967.
(76) Ceulemans, A.; Vanquickenborne, L. G. *J. Am. Chem. Soc.* **1981**, *103*, 2238.

Table 6. Fragment Analysis for the Frontier Molecular Orbitals in Ir(bib)(mppy)Cl at X-ray Structure Using the ADF 2002 Program Package[a]

MO	major contribution of fragment orbital (%)
	Unoccupied
LUMO+2	bib-65* (59), ppy-34* (24), $5d_{yz}$ (4.0), bib-68* (2.1)
LUMO+1	ppy-33* (80), ppy-34* (9.2), ppy-32 (3.6), $5d_{xz}$ (2.7)
LUMO	bib-64* (82), bib-63 (11), $5d_{xy}$ (2.7)
	Occupied
HOMO	$3p_x$ (48), $5d_{xy}$ (33), ppy-31 (6.9), bib-61 (5.3), bib-64* (1.4)
HOMO-1	$3p_z$ (60), $5d_{yz}$ (23), bib-62 (3.8), bib-68* (1.4), bib-65* (1.3)
HOMO-2	$3p_x$ (29), bib-61 (19), $5d_{xz}$ (16), $5d_{xy}$ (13), ppy-31 (6.0), bib-60 (4.1), ppy-30 (2.5), bib-57 (2.3), bib-58 (2.0)

[a] The * denotes unoccupied orbital.

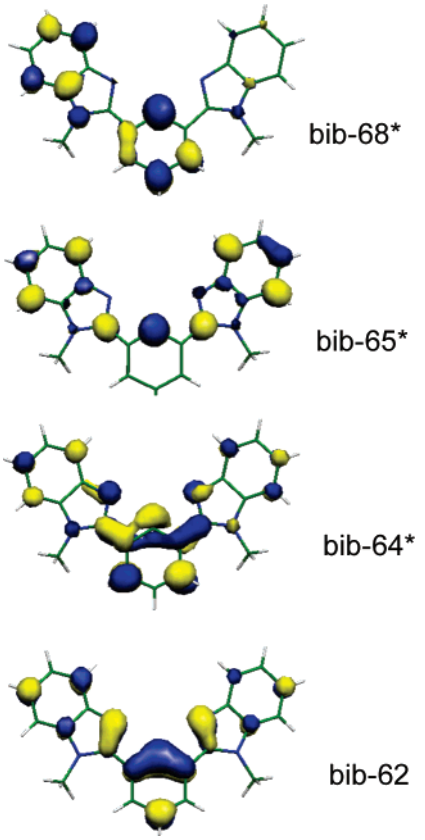

Figure 10. Molecular orbitals involved in the interligand transition ascribed to the intensity of the S_2 transition in Ir(Mebib)(mppy)(Cl).

symmetry. The CT transition in S_2 is therefore borrowed intensity from interunit transitions. Because HOMO-1 has the contribution of both the occupied bib-62 and unoccupied bib-65*, the CT transition can borrow intensity from both bib-62 → bib-64* and bib-65* → bib-64* intra-Mebib transitions. As shown in Figure 10, bib-64* contains the π^* orbitals on two benzimidazoyl (bim) moieties with out-of-phase combination, while the π orbitals are combined in an in-phase fashion in bib-62. Therefore, the electronic transition bib-62 → bib-64* generates a strong electronic oscillator between two π systems of bim moieties approximately 10 Å apart. Similarly, bib-65* involves an in-phase interaction between the π^* orbitals of bim moieties; therefore, the transition between unoccupied orbitals bib-65* → bib-64* also produces a large transition dipole moment. The direction of the dipole moment of both intra-bib transitions is along the inter-bim direction, which is the *x* axis, consistent with the results obtained by TDDFT.

Consequently, the theoretical consideration based on DFT calculations revealed that the intense phosphorescence of the Ir−Mebib complexes is accounted for in terms of the effective mixing between the $5d_{xy}$ → LUMO configuration in the lowest triplet state with $5d_{yz}$ → LUMO in singlet states through spin−orbit coupling. In addition, the intensity of the singlet $d\pi^*$ transition originates from the very unique electronic structure of Mebib, which allows for an electronic interaction between the spatially separated bim moieties.

Conclusion

In the present study, we achieved the selective synthesis of novel mixed-ligand Ir complexes of the general formula [Ir(N∧C∧N)(ppy)X] (N∧C∧N = Me- or Phbib; X = Cl, Br, I, −CCPh, or CN), which have high luminescent quantum yields, $\Phi = 0.77 \sim 0.95$. The X-ray structures of [Ir(Phbib)(ppy)Cl] and [Ir(Mebib)(mppy)Cl] ′reveal that the nitrogen atom in the ppy ligand is located at a position trans to the central carbon atom in N∧C∧N (Me- or Phbib), while the coordinating carbon atom in ppy occupies a trans position in relation to Cl. Upon a change of substituent on ppy or X, the Ir(III/IV) oxidation potential exhibits a strong dependence on the ligand substitution, although the reduction potentials remain almost constant. These findings suggest that the excited state involves a large contribution of MLCT character, which is supported by DFT calculations. Therefore, the present Ir(bib) complexes provide new insight into the molecular design of a new type of highly emissive phosphorescent Ir complexes. Investigation of Ir(III) complexes with regard to this concept is now in progress.

Acknowledgment. M.H. gratefully acknowledges financial support from the Institute of Science and Engineering at Chuo University, the Ministry of Education, Science, Sports, and Culture (Monkasho) for a Grant-in-Aid for Scientific Research (No. 15310076 and 16074215 "Chemistry of Coordination Space"). K. N. gratefully acknowledges Monkasho for a Grant-in-Aid for Scientific Research (16550056).

Supporting Information Available: CIF files of **5**·$2CH_2Cl_2$, **9**·C_6H_{14}, **11**OTf·Et_2O, **13**OTf, and **14**PF_6·2MeCN·$0.5Et_2O$, and Tables 1S and 2S give their selected bond distances and angles and the torsion angles between planes. Tables 3S, 4S, and 5S summarize the excitation energy, oscillator strength (f), and major electronic configurations for Ir(Mebib)(mppy)Cl (**5**), Ir(Mebib)(ppy)$(CH_3CN)^+$ (**11**), and Ir(Mebip)(ppy)Cl^+ (**14**). This material is available free of charge via the Internet at http://pubs.acs.org.

IC060796O